Energy 303 (2024) 131437

Contents lists available at ScienceDirect

Energy

journal homepage: www.elsevier.com/locate/energy

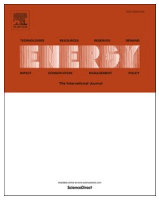

Study on performance of direct-expansion heat pump water heater integrated uninsulated micro-channel PV/T solar collector

Lidong Yang [a], Qiang Gao [a], Qiang Xu [a], Liwei Yang [b,c], Rongji Xu [a,*], Hongbing Chen [a], Huasheng Wang [b]

[a] Beijing Engineering Research Center of Sustainable Energy and Buildings, Beijing University of Civil Engineering and Architecture, Beijing, 100044, China
[b] School of Material Science and Engineering, Queen Mary University of London, London, E1 4NS, UK
[c] School of Energy and Power Engineering, Beihang University, Beijing, China

ARTICLE INFO

Keywords:
Uninsulated micro-channel PV/T
Coefficient of performance
Heat pump
Solar energy
Photovoltaic

ABSTRACT

In this paper, a direct-expansion heat pump water heater system integrated uninsulated micro-channel PV/T solar collector (UMC-PVT-SC) is proposed. This system can realize storage for both thermal energy and electricity, ensuring the supply of domestic hot water. The theoretical models of micro-channel PV/T solar collector, hot water storage tank, compressor and electronic expansion valve are established to investigate the performance of the micro-channel PV/T heat pump water heater system. R134a is used as refrigerant. The system performance is numerically simulated using MATLAB for different solar radiation intensity, ambient temperature and wind speed. The results show that solar radiation intensity has the largest influence on the system performance, followed by ambient temperature and wind speed. The coefficient of performance of the heat pump (COP_{HP}) and the overall coefficient of performance (COP_{pvt}) of the integrated system increase while the required operating time reduces, as solar radiation intensity and ambient temperature increase. The uninsulated micro-channel PV/T solar collector (evaporator) can absorb thermal energy from both ambient air and solar radiation and therefore achieve high COP_{HP}, electric efficiency and COP_{pvt}. Even under cold weather conditions, the proposed solar collector and heat pump heater demonstrate high efficiencies, heating and power generation capacities. When ambient temperature is −18.6 °C and solar irradiance is 322 W/m^2, the collector efficiency and electric efficiency of UMC-PVT-SC are still at 0.718 and 0.244, respectively, and the COP_{HP} and COP_{pvt} of the heat pump heater are 3.5, 5.63, respectively. The present work is of potential value for delivering net zero.

1. Introduction

At present, in the face of global energy crisis and climate change [1], renewable energy has become the common choice of the world [2] to achieve carbon emission reduction. Solar energy has become a reliable choice because of its advantages of clean, large reserves and easy availability.

As a highly-efficient energy-saving device, heat pump can make full use of low-grade thermal energy and plays an important role in many applications. The integration of heat pump and solar collector can improve the coefficient of performance (*COP*) of heat pump and the utilization rate of solar energy. Direct-expansion solar-assisted heat pump (DX-SAHP) systems, which use the solar collector as the evaporator of the heat pump systems, have attracted much attention because of their simplicity, reliability and high efficiency. Moreno-Rodriguez et al. [3] carried out experimental verification on a DX-SAHP system from the aspects of outdoor temperature, solar irradiance, wind speed. The results showed that under the extreme outdoor conditions where the collector is covered with snow and the experimental condensation temperature reached 32 °C, the system *COP* can be maintained between 1.9 and 2.7, which can maintain the thermal energy required by the compensation system. Sun et al. [4] analyzed the performance of conventional air source heat pump water heater (ASHPWH) and direct expansion solar-assisted heat pump water heater (DX-SAHPWH) under different operating conditions by means of experiments and simulations. The results showed that the *COP* of DX-SAHPWH was obviously higher than that of ASHPWH in sunny days, but the performance of DX-SAHPWH was poor in nights because of the poor convective heat transfer performance of solar collectors. Song et al. [5,6] proposed a novel direct-expansion heat pump with a hybrid compound parabolic

* Corresponding author.
E-mail address: xurongji@bucea.edu.cn (R. Xu).

https://doi.org/10.1016/j.energy.2024.131437
Received 23 December 2023; Received in revised form 20 March 2024; Accepted 24 April 2024
Available online 29 April 2024

concentrator/photovoltaic/fin evaporator. The established system can make full use of solar and air energies in a limited space to achieve a much higher unit output. Results show that the solar irradiance and wind speed are beneficial for the coefficient of performance, but the water temperature is not. In the absence of solar radiation, the performance coefficient of the system can reach 4.08. Kong et al. [7–9] conducted a series of studies on the effects of different compressor operating states, refrigerant types, and meteorological parameters on DX-SAHP system performance by combining system simulation and experimentation, indicating that the deceleration mode of the compressor speed can stabilize the compressor power and improved the average *COP* of the system, and the acceleration mode could stabilize the evaporating temperature; Under the same test conditions, R290 DX-SAHP system has higher performance coefficient and heat collection efficiency than R134a system. Meteorological parameters have a great influence on the thermal performance of the DX-SAHP system, the *COP* of the system increase, while the required heating time reduces, as solar radiation intensity and ambient temperature increase. Rabelo et al. [10] studied the economically optimum size of collector area for the DX-SAHP under different weather conditions, and the influence of the weather conditions, the refrigerant, the costs and the heating capacity on the payback period and optimum collector size. Zhang et al. [11] built and tested a solar-air composite heat source heat pump (SA-CHSHP) in outdoor dynamic environment, the results showed that the *COP* of the system in autumn can reach a maximum of 4.8, which is still higher than 2.7 even in cloudy days, in winter, the *COP* can also be maintained between 2.87 and 3.8, and it can run stably under various working conditions. Yang et al. [12–14] studied the solar-assisted air source heat pump in detail, and made a comprehensive overview and analysis of the current research progress of the solar-assisted air source heat pump, concluded that solar-assisted air source heat pumps have great prospects in the field of space heating and heat pumps and the high-efficiency solar collectors, as the core components of direct expansion solar heat pumps, have a great impact on the performance of the system. On the other hand, combining the photovoltaic cell with the evaporative thermal absorber of the direct-expansion heat pump system can not only achieve the effect of utilizing both photovoltaic and photothermal, but also reduce the temperature of photovoltaic cell and improve its power generation efficiency.

Therefore, high efficiency PV/T module is the key to improve the performance of DX-SAHP. The PV/T component is integrated by the PV plate and evaporator, where the flat-plate tube structure is typical of the evaporator, usually, the copper coil is welded to the metal base plate and bonded to the back of the PV plate [15]. Many scholars have conducted extensive research on heat pump systems composed of above structure. Abbas et al. [16] designed a series-coupled PV/T and solar TC with direct expansion heat pump system and performed performance simulations and experimental study. The average daily electrical efficiency, collector efficiency and total efficiency of the system are 14.1 %, 60.1 % and 74.2 %, respectively. Cai et al. [17] proposed a novel PV/T-air dual source heat pump water heater (PV/T-AHPWH), a PV/T evaporator and an air source evaporator are connected in parallel and operate simultaneously. The maximum collector efficiency of the PV/T evaporator was 78.7 %, the maximum electric efficiency was 15.5 %, and the maximum overall efficiency was 117.4 %. The arrangement of metal base plates and copper coils in the flat-plate tube structure increases the weight of the PV/T component, limiting its application in the project. Roll-bond technology is also widely employed for the manufacturing of evaporator. Its processing technology is to embed the fluid channel between two rolled plates, design the flow channel form and distribution according to the requirements [18]. Lu et al. [19] designed a vapor injection PV/T heat pump system based on roll-bond evaporator and conducted thermodynamic comparative analysis with an ideal conventional vapor compression cycle verifying the advantages of applying VI cycle. The average collector efficiency and electric efficiency of the proposed system are 49.9 % and 7.5 %, respectively. However, the roll-bond evaporator typically has a large area and weak pressure capacity due to size and process limitations. Operating under high temperature conditions in summer can easily lead to tube explosion, and the long-term reliability and corrosion risk problems need to be solved. As a heat transfer element with extremely high thermal conductivity, heat pipes can be combined with PV panels to integrate heat pipe solar PV/T collectors, which is a solution to improve system performance. In PV/T modules, the choice of solar collector is crucial. Chen et al. [20,21] proposed a heat pipe PV/thermal (PV/T) heat pump system and compared the system performance of PV/T panel and traditional PV panel. The electric efficiency of PV/T panel is improved relatively by 25.7 % and 14.2 % compared with traditional PV panel under the heating mode and heat charging mode, respectively; at the same time, six working modes are proposed and discussed to investigate the effect of meteorological parameters, PV panel parameters, and heat pipe pitch on the performance of the heat pipe PV/T heat pump system.

Micro-channel heat exchangers have been widely used due to their high heat transfer efficiency and compactness [22]. Flow boiling heat transfer of refrigerants in micro-channels is much higher compared with that in larger diameter round tubes [23]. Therefore, micro-channel solar collectors (MSC) can have higher collector efficiency, smaller volume and weight. It also reduces manufacturing costs [24]. At the same time, MSC adopts the structure of plane surfacing, so that it can be well combined with photovoltaic modules. In recent years, the research of integrating micro-channel PV/T solar collector (MC-PVT-SC) by combining MSC with photovoltaic module has attracted much attention. Zhou et al. [25] built a solar direct-expansion heat pump system using a MC-PVT-SC, attached the micro-channel to the photovoltaic module and installed an insulation layer, and carried out theoretical and experimental studies on the collector efficiency, electric efficiency, overall efficiency and *COP* of the system under real-time operation conditions. The results of these parameters were 55 %, 13.7 %, 69.1 % and 5.0, respectively. Zhang et al. [26] proposed a novel dual-mode heat pump with a hybrid PV/micro-channel heat pipe/fin heat exchanger and conducted a simulation study on the heating and cooling performance of the system. Results show that the novel system demonstrates an excellent performance, especially improving the cooling and electrical capacity in the clear summer day. On a typical winter day, its mean heating capacity, electricity generation, and coefficient of performance are 1756 W, 148.6 W, and 5.28, respectively. Modjinou et al. [27] employed micro-channel heat pipes to enhance heat transfer within the PV/T system, effectively reducing the temperature of PV panels. Their results indicate that the average collector efficiency, average electrical efficiency, and combined efficiency of the PV/T system based on micro-channel heat pipes are 27.75 %, 7.78 %, and 35.53 %, respectively.

Currently, the MC-PVT-SC for direct-expansion heat pumps mainly adopt the thermal insulation layer which can reduce the heat loss from photothermal conversion process to a certain extent, but it reduces the thermal energy absorbed by the micro-channel evaporator from ambient air. The usual approach to enable the system to operate without solar radiation is to add an additional air-source evaporator. In this paper, a micro-channel evaporator is pressed under the photovoltaic component to form the MC-PVT-SC of direct-expansion heat pump, and no insulation layer is added. It is an innovative method. The uninsulated micro-channel PV/T solar collector (UMC-PVT-SC) can absorb thermal energy from both ambient air and solar radiation. Therefore, the DX-HPWH system integrated UMC-PVT-SC exhibits a higher energy utilization rate and enhanced environmental adaptability compared to the traditional direct-expansion PVT solar heat pump system. By employing photovoltaic power as the driving force for the compressor, this system reduces its reliance on the grid, making it a viable solution for remote areas or locations with unstable power supply. The theoretical model of the DX-HPWH system integrating UMC-PVT-SC is established, and the influences of this novel structure PV/T component and meteorological parameters (solar radiation intensity, ambient temperature and wind

speed) on system performance are studied. The findings of the study will contribute to the advancement of novel, low-carbon, and high-efficiency solar heat pump systems.

2. Design and modeling of the uninsulated micro-channel-PVT-solar collector

The key component of the system investigated is the UMC-PVT-SC which provides both thermal energy and electricity to the system. The electricity is used to drive the DC compressor and the thermal energy is used as the heat source of the heat pump. When the evaporation temperature of the heat pump cycle is lower than the ambient temperature, the UMC-PVT-SC can simultaneously absorb both solar energy and ambient thermal energy. During nighttime, the system works as an air source heat pump.

Figs. 1 and 2 show the physical model of the UMC-PVT-SC, including frame, glass, PV cell, EVA film, TPT film and the micro-channel flat tube evaporator attached to the bottom. The incident solar radiation energy on the surface of the PV panel is converted into electrical energy by photovoltaic cells. EVA film and TPT film are Ethylene-vinyl acetate and Tedlar-Polyester-Tellar, respectively. The EVA film and TPT film bond the layers of photovoltaic modules together. The micro-channel evaporator consists of multiple parallel aluminum micro-channel flat tubes, securely bonded to the TPT layer using thermally conductive silica gel. The ends of each flat tube are connected to the refrigerant's distributing tube and collecting tube, while each flat tube contains numbers of rectangular micro-channels (1mm × 1 mm) for fluid flow. To make use of thermal energy from ambient air, no insulation is employed to the solar collector. Micro-channel solar collector is used as evaporator to absorb thermal energy from both PV panel and ambient air. Consequently, the heat pump system operates seamlessly in the presence or absence of sunlight, utilizing the PV/T component solely without the need for an additional air-source evaporator. In addition, the micro channel can reduce the temperature of PV modules and improve its efficiency of power generation.

To ensure that the system meets energy efficiency and reliability requirements under typical operating conditions, system design parameters are determined through cyclic thermodynamic calculations and actual load demands. The system aims to provide users with 100 L of domestic hot water daily, with a water tank heating time of 3 h. This represents the heat load of the system. Based on typical meteorological conditions in Beijing, appropriate temperature differentials for heat exchange on both the micro-channel evaporator and condenser sides were selected to determine the operating parameters of the heat pump cycle, including evaporating temperature, condensing temperature, superheat, subcooled, and to calculate the theoretical heating capacity and coefficient of performance (*COP*) of the cycle. Design parameters for the compressor and micro-channel evaporator were determined based on the thermodynamic calculation results. The determination of the PV panel considered the electricity conversion efficiency of the panel and the power consumption of the compressor, ensuring that the system can drive the compressor under different weather conditions and operate normally. The selection of appropriate micro-channel flat tube spacing and number was based on the theoretical heat transfer area of the micro-channel evaporator, aiming to achieve seamless integration with the PV panel for optimal overall performance. The detailed design parameters for system components are given in Tables 1 and 2.

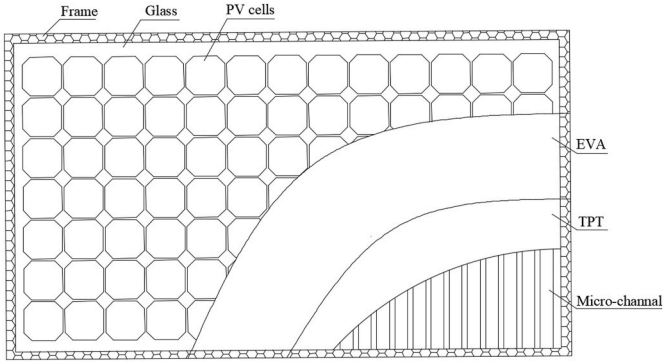

Fig. 1. Structure diagram of UMC-PVT-SC.

2.1. Model for the thermal energy conversion process of the micro-channel evaporator

The model of the micro-channel evaporator is constructed based on the following assumptions. The flow of refrigerant in each micro-channel of evaporator and condenser is assumed as one-dimensional flow. Within the same small element, the quantities such as refrigerant temperature and dryness, the internal and external wall temperatures of the micro-channel are regarded as the same. The pressure drops of refrigerant flow in evaporator, condenser, and pipes are ignored.

Taking 1 kJ/kg as the unit, the differential element division of equal enthalpy difference is carried out. The heat absorbed by the refrigerant in the *i*-th micro-channel element, $Q_{ev,i}$, can be calculated by Eq. (1):

$$Q_{ev,i} = m_{r,i}\left(h_{ev,out,i} - h_{ev,in,i}\right) \tag{1}$$

The flow and heat transfer of refrigerant in the micro-channel evaporator tube is divided into superheated and two-phase zones. In the superheated zone, the criterion formula is adopted as Gnielinski correlation, which can be expressed by Eq. (2)[28]:

$$Nu_f = \frac{(f/8)(Re_f - 1000)Pr_f}{1 + 12.7\sqrt{f/8}\left(Pr_f^{2/3} - 1\right)}\left[1 + \left(\frac{D}{l}\right)^{2/3}\right]\left(\frac{T_f}{T_{wl}}\right)^{0.45} \tag{2}$$

The f is the friction factor, which can be calculated by Filonenko correlation as Eq. (3):

$$f = \left(1.82 \lg Re_f - 1.64\right)^{-2} \tag{3}$$

In the two-phase zone, the refrigerant condensation heat transfer coefficient h_{tp} is calculated using the correlation proposed by Fang [29] based on the experimental database. The dimensionless numbers are defined as the following:

$$h_{tp} = \frac{Nu\lambda_L}{D} \tag{4}$$

$$Nu = F_f M^{-0.18} Bo^{0.98} Fr_{lo}^{0.48} Bd^{0.72}\left(\frac{\rho_L}{\rho_G}\right)^{0.29}\left[\ln\left(\frac{\mu_{lf}}{\mu_{lw}}\right)\right]^{-1} Y \tag{5}$$

$$Y = \begin{cases} 1 & \text{for } p_r \le 0.43 \\ 1.38 - p_r^{1.15} & \text{for } p_r > 0.43 \end{cases} \tag{6}$$

where p_r is the reduced pressure, $p_r = p/p_{crit}$, Bo is the boiling number, $Bo = q/Gh_{lg}$, Fr_{lo} is the liquid only Froude number, $Fr_{lo} = G^2/gD\rho_L^2$, D is the hydraulic diameter, $D = 4A_c/P$, Bd is the Bond number, $Bd = g(\rho_L\text{-}\rho_G)D^2/\sigma$.

2.2. Model of the electricity generation of the PV cell

The incident solar irradiance on the surface of the PV cell undergoes energy loss due to reflection. One part of the remaining energy is converted into electricity, and the other part is turned into heat raising the temperature of the PV cell. The heat is transferred to the top of the glass and the bottom of the TPT by heat conduction, and then diffused by convection and radiation. The energy transfer process is shown in Fig. 3.

The energy balance equation of PV cell can be expressed as Eq. (7):

$$A_{pv,i}\tau_g\alpha_{pv}I - A_{pv,i}E_i - Q_{rad,i} - Q_{convpv,i} - Q_{pv,i} = 0 \tag{7}$$

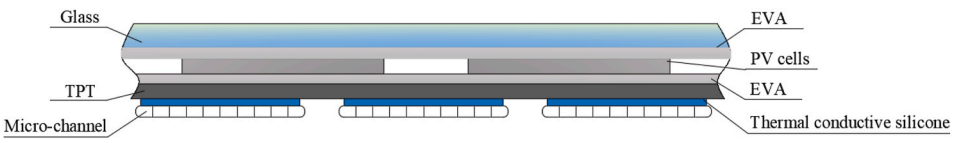

Fig. 2. Schematic diagram of partial section structure of UMC-PVT-SC.

Table 1
Components selected for the system.

Component	Type	Remarks
Compressor	BSG133SKE	Refrigerants: R134a Rated voltage: 48 V DC Rated Speed: 3000 rpm Displacement volume: 13.3 cm^3/rev
Hot water storage tank	Pressure resistance and heat insulation	100 L water, micro-channel condenser is wrapped around the hot water storage tank
Photovoltaic module	TSM-410DE15H (II)	Maximum power: 410 W ± 3 % Maximum power voltage: 41.7 V Maximum power current: 9.84 A
Electronic expansion valve	DPF (Q01) 1.3	Inner diameter 1.3×10^{-3} m

where, the power of the PV cell E is related to solar radiation intensity I and PV cell temperature, and can be expressed by Eq. (8)[30]:

$$E_i = A_{pv} I \eta_{rc} \left(1 - \beta_{rc}\left(T_{pv,i} - T_{rc}\right)\right) \tag{8}$$

2.3. Model of the UMC-PVT-SC

The convective heat transfer coefficient of the upper surface of the glass and the lower surface of the micro-channel and TPT layer can be calculated by Eq. (9)[31]:

$$h = 2.8 + 3u_w \tag{9}$$

The radiation heat transfer between the upper surface of the glass and the sky is calculated by Eq. (10)[32]:

$$Q_{rad,i} = \varepsilon_g \sigma A_{g,i}\left(T_{sky}^4 - T_{g,i}^4\right) \tag{10}$$

The effective sky temperature T_{sky}, is determined by Eq. (11)[33]:

$$T_{sky} = 0.0553 T_a^{1.5} \tag{11}$$

According to energy conservation, the heat absorption of UMC-PVT-SC can be expressed by Eq. (12):

$$Q_{ev,i} = Q_{pv,i} + Q_{b,i} \tag{12}$$

The heat transfer process on the upper surface of the micro-channel tube is shown in Fig. 4. The heat $Q_{pv,i}$ can be calculated by Eq. (13):

$$Q_{pv,i} = \left(t_{pv} - t_{r,i}\right) \Big/ \left(\frac{\delta_{EVA}}{\lambda_{EVA} A_{EVA,i}} + \frac{\delta_{TPT}}{\lambda_{TPT} A_{TPT,i}} + \frac{\delta_{tcs}}{\lambda_{tcs} A_{tcs,i}} + \frac{\delta_{em}}{\lambda_{em} A_{owe,i}} \frac{1}{h_{r,i} A_{iwe,i}}\right) \tag{13}$$

The heat transfer process on the lower surface of the micro-channel tube is shown in Fig. 5. The heat $Q_{b,i}$ can be calculated by Eq. (14):

$$Q_{b,i} = \left(t_a - t_{r,i}\right) \Big/ \left(\frac{1}{h_{r,i} A_{iwe}} + \frac{\delta_{em}}{\lambda_{em} A_{iwe}} + \frac{1}{h_{b,em} A_{owe}}\right) \tag{14}$$

The heat absorption of UMC-PVT-SC can be expressed by Eq. (15):

$$Q_{ev} = \sum_{i=1}^{n} Q_{ev,i} \tag{15}$$

Table 2
Parameters used in the modeling and simulation of the system.

Component	Parameters	Value
Condenser	Distance between micro-channels (H)	0.002 m
	Slices	20
	Number of runners	12
	Length of monolithic micro-channel	1.3 m
	Width of monolithic micro-channel (y)	0.025 m
	Height of monolithic micro-channel (s)	0.002 m
	Runner length of monolithic micro-channel	1.3 m
	Runner width of monolithic micro-channel	0.001 m
	Runner height of monolithic micro-channel (δ_{cm})	0.001 m
	Thermal conductivity of aluminum (λ_{cm})	237 W/(m·K)
	Insulation factor (Af_{tk})	0.95
	Hydraulic diameter (D)	0.001 m
Hot water storage tank	Maximum capacity	120 L
	Contact thermal resistance between storage tank and micro-channel	2.5×10^{-6} $(m^2\ K)/W$
	Thermal conductivity of hot water storage tank inner shell (λ_{tk})	36 W/(m·K)
	Wall thickness of hot water storage tank inner shell (δ_{tk})	0.002 m
Evaporator	Distance between micro-channels (H)	0.017 m
	Slices	13
	Number of runners	15
	Length of monolithic micro-channel	1.9 m
	Width of monolithic micro-channel (y)	0.05 m
	Height of monolithic micro-channel (s)	0.002 m
	Runner length of monolithic micro-channel	1.9 m
	Runner width of monolithic micro-channel	0.001 m
	Runner height of monolithic micro-channel (δ_{em})	0.001 m
	Thermal conductivity of aluminum (λ_{em})	237 W/(m·K)
Photovoltaic module	Thermal conductivity of glass (λ_g)	0.98 W/(m·K)
	Thermal conductivity of TPT film (λ_{TPT})	0.61 W/(m·K)
	Thermal conductivity of EVA film (λ_{EVA})	0.23 W/(m·K)
	The thickness of EVA film (δ_{EVA})	0.0005 m
	The thickness of glass (δ_g)	0.003 m
	The thickness of TPT film (δ_{TPT})	0.0001 m
	The thickness of glass (δ_g)	0.001 m
	Thermal conductivity of EVA film (λ_{EVA})	2 W/(m·K)
	Surface emissivity of glass (ε)	0.8
	Light transmittance of glass (τ_g)	0.89
	Absorption rate of photovoltaic cells (α_{pv})	0.98
	The temperature coefficient (β_{rc})	0.0045 K^{-1}
	The electrical efficiency of PV under standard condition (η_{rc})	0.204
	Photovoltaic cell area (A_{pv})	1.88 m^2
	Photovoltaic module area (A_{pvt})	2 m^2

3. DX-HPWH system based on UMC-PVT-SC

The DX-HPWH system based on UMC-PVT-SC is mainly composed of UMC-PVT-SC, micro-channel condenser, hot water storage tank, electronic expansion valve, Maximum Power Point Tracking controller (MPPT), battery, relay and DC compressor, as shown in Fig. 6. The system uses R134a as refrigerant. The refrigerant in the UMC-PVT-SC absorbs energy from both solar radiation and ambient air. After being compressed by the compressor, the high-pressure and high-temperature refrigerant releases heat in the micro-channel condenser to the water in the hot water storage tank. Then the refrigerant is expanded in the electronic expansion valve and re-enters the UMC-PVT-SC to absorb heat. The UMC-PVT-SC absorbed energy ratio of solar to air is

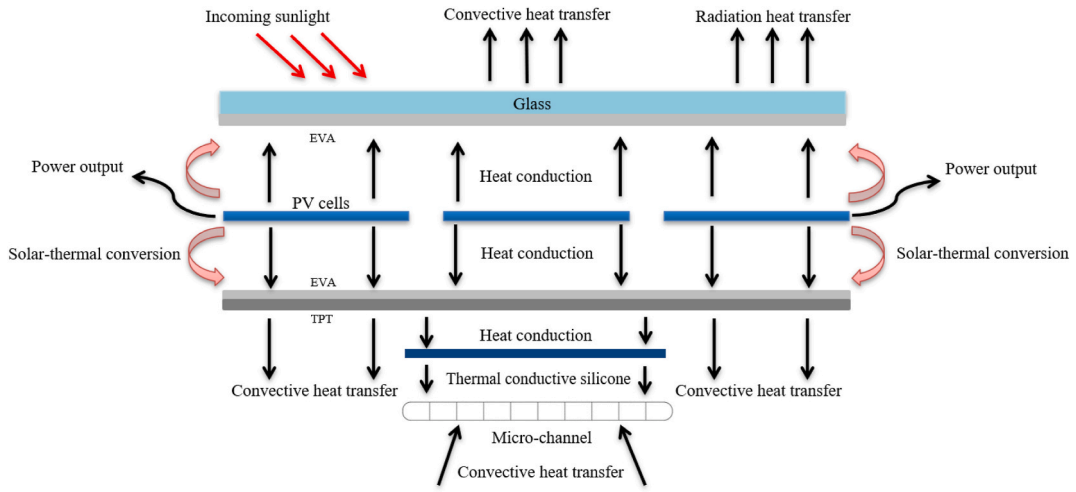

Fig. 3. Energy transfer process in UMC-PVT-SC.

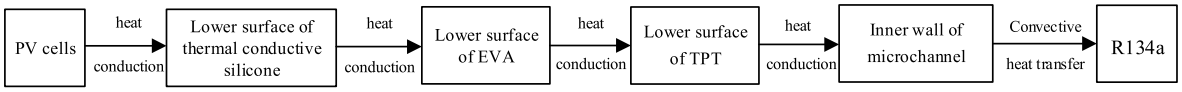

Fig. 4. Heat transfer process on the upper surface of UMC-PVT-SC.

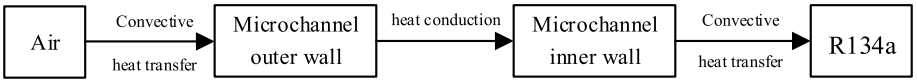

Fig. 5. Heat transfer process on the lower surface of UMC-PVT-SC.

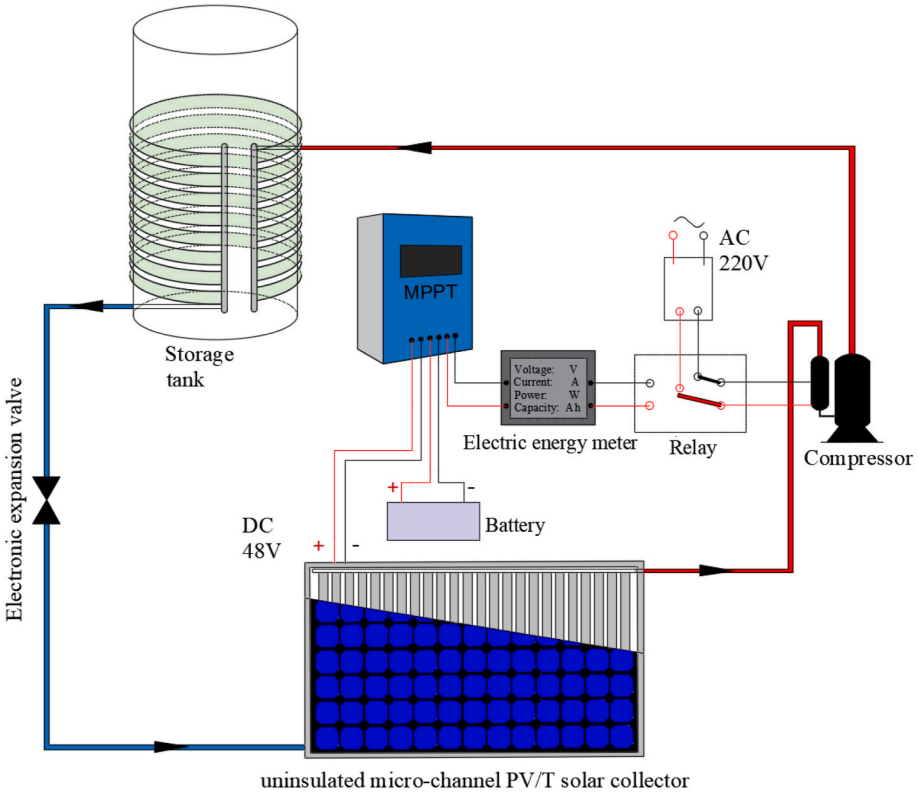

Fig. 6. Schematic of the heat pump water heater integrating uninsulated micro-channel PV/T solar collector.

dynamically adjusted by the change of the evaporation temperature of the heat pump system. In the PV part, the short-wave part of the solar radiation is converted into electricity by PV modules, adjusted by the MPPT controller. The generated electricity is stored in the battery and then used by the DC compressor of the heat pump system. When the stored battery power is insufficient, the electricity from the mains grid is used to drive the system. Compared with the conventional air source heat pump water heater, the system investigated in this paper uses the UMC-PVT-SC as evaporator without copper tubes, which achieves both high efficiency energy utilization and low cost.

In photovoltaic/utility control systems, the use of an energy meter alone can monitor the voltage and quantity of lithium batteries. When combined with a relay battery outage control module, the lower limit voltage is set based on the charging and discharging characteristics of the lithium battery and the range that meets the normal working voltage of the compressor to control the discharge of the lithium battery. 220 V AC mains power is converted into 48 V DC power through a rectifier and connected to an intermediate relay. The electric energy meter is connected in series with the discharge circuit of the lithium battery. The current output by the lithium battery is monitored by the electric energy meter and connected to the intermediate relay. When the voltage of the lithium battery fed back to the relay by the electric energy meter is lower than the lower limit voltage, the relay path is disconnected, that is, the discharge path of the lithium battery is disconnected. At that time, the electricity from the mains grid drives the compressor. When the voltage of the lithium battery reaches 48 V after photovoltaic charging, the power supply is automatically switched to the lithium battery. This enables controllable switch of photovoltaic/mains power supply.

To predict the operation performances of the heat pump water heater system under different meteorological conditions, theoretical models of the components and the system are built to describe the working processes of the system. The thermophysical properties of water and refrigerant are obtained from REFPROP 10.0. The performance indicators such as evaporation temperature/pressure, condensation temperature/pressure, capacity of evaporator/condenser and *COP* are used to analyze system performance under different working conditions.

The following assumptions are made for the establishment of the system model:

1. The system operates at steady-state.
2. The water temperature in the hot water storage tank is uniform without temperature stratification.
3. The compression process of refrigerant in the compressor is regarded as a polytropic process.
4. The expansion process of refrigerant in the electronic expansion valve is regarded as an isenthalpic process.
5. The contact thermal resistances between the layers of PV/T components are neglected.

3.1. Compressor model

The compressor drives the refrigerant flowing in the heat pump system. To match the real compression process, the operation parameters of the compressor under different working conditions are taken from the real performance curve of the compressor (from Product manual), as shown in Figs. 7 and 8. When the operating point is between the curves, the linear interpolation method is used to obtain the value, so the calculation of the theoretical model of the system can be close to the real situation and the practical operation performance of the system can be better reflected.

3.2. Hot water storage tank model

Fig. 9 shows the schematic of hot water storage tank. The high-temperature and high-pressure refrigerant flows through the micro-channel condenser and transfers heat to the water stored in the storage tank, raising the water temperature. The heat transfer process of refrigerant in micro-channel condenser is divided into several small elements in the model of hot water storage tank.

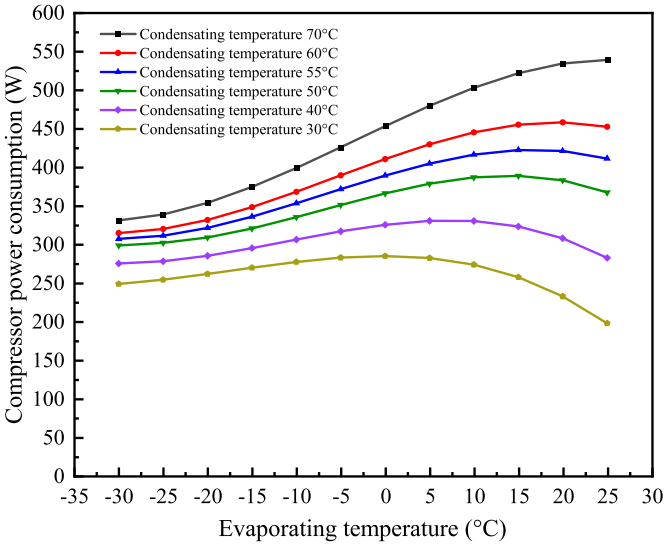

Fig. 7. Curve for the electricity consumption of compressor.

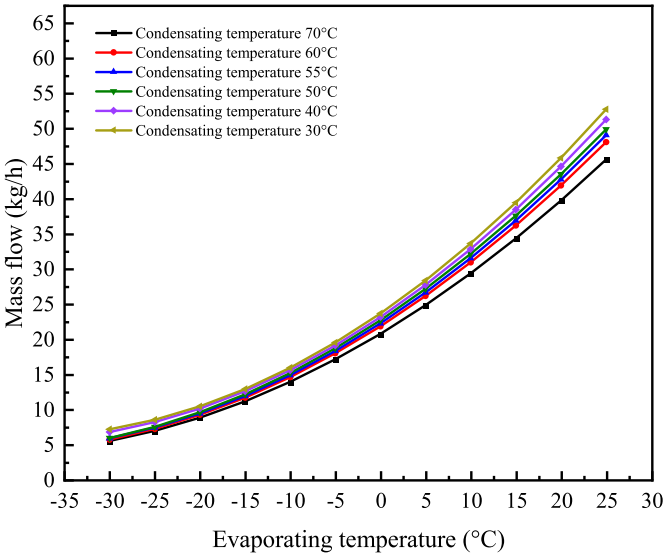

Fig. 8. Curve for the mass flow rate of compressor.

Similar to the calculation for the micro-channel evaporator of the UMC-PVT-SC, taking 1 kJ/kg as the unit, the differential element division of equal enthalpy difference is carried out. The heat transfer rate $Q_{con,i}$, released by the refrigerant in the *i*-th micro-channel element can be calculated by Eq. (16):

$$Q_{con,i} = m_{r,i}\left(h_{con,in,i} - h_{con,out,i}\right) \tag{16}$$

The correlation of convective heat transfer on the water side of the hot water storage tank [34] is calculated by Eq. (17):

$$Nu_{w,i} = 0.59\left(Gr_{w,i}Pr_{w,i}\right)^{0.25} \tag{17}$$

where, $Gr_{w,i}$ is the Grashof number of water in the storage tank in the *i*-th division element, which can be calculated by Eq. (18):

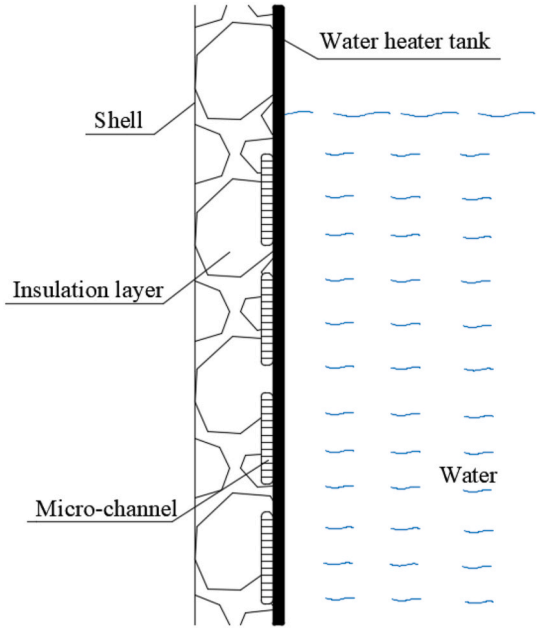

Fig. 9. Schematic of hot water storage tank.

$$Gr_{w,i}=\frac{g\alpha_{w,i}\left(t_{r,i}-t_w\right)l_i^{\,3}}{{\nu_{w,i}}^2} \tag{18}$$

$Pr_{w,i}$ is the Prandtl number of water in the storage tank in the i-th division element, which can be calculated by Eq. (19):

$$Pr_{w,i}=\frac{\nu_{w,i}}{a_{w,i}} \tag{19}$$

Then the convective heat transfer coefficient on the water side of the hot water storage tank is defined as (Eq. (20)):

$$h_{w,i}=\frac{Nu_{w,i}\lambda_{w,i}}{l_i} \tag{20}$$

The heat transfer process between refrigerant and hot water is shown in Fig. 10, and the heat transfer of each small element can be expressed by Eq. (21):

$$Q_{con,i}=\left(t_{r,i}-t_w\right)\Big/\left(\frac{1}{h_{r,i}A_{iwc}}+\frac{\delta_{cm}}{\lambda_{cm}A_{owc}}+\frac{\delta_{tk}Af_{tk}}{\lambda_{tk}A_{owt}}+\frac{Af_{tk}}{h_{w,i}A_{iwt}}+R\right) \tag{21}$$

In fact, only one side of the micro-channel condenser is involved in heat transfer, and the heat transfer model can be simplified to the heat transfer through fins. The micro-channel structure is shown in Fig. 11. The fin efficiency is calculated by Eq. (22):

$$F=\frac{th(nH)}{nH} \tag{22}$$

where, n can be calculated by Eq. (23):

$$n=\sqrt{\frac{2h_{r,i}}{\lambda_{cm}\delta_{cm}}} \tag{23}$$

The calculation for the heat transfer in the micro-channel condenser is different from that in the micro-channel evaporator. Gnielinski formula [28] is used in the single-phase zone. In the superheated zone, the calculation is the same as that for the evaporator. In the subcooled zone,

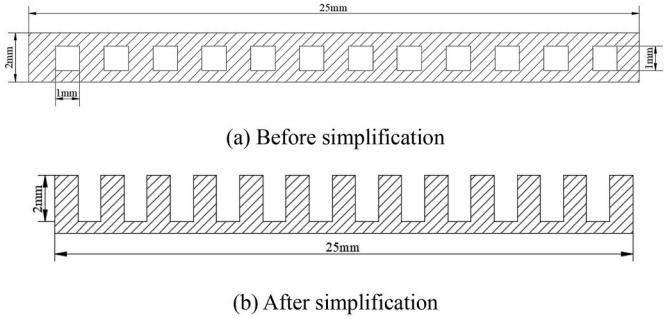

Fig. 11. The structure of micro-channels.

the correlation can be expressed as Eq. (24):

$$Nu_f=\frac{(f/8)(Re_f-1000)Pr_f}{1+12.7\sqrt{f/8}\left(Pr_f^{2/3}-1\right)}\left[1+\left(\frac{D}{l}\right)^{2/3}\right]\left(\frac{Pr_f}{Pr_{wl}}\right)^{0.01} \tag{24}$$

The correlation of Jige et al. [35] is selected to calculate the heat transfer of refrigerant in the two-phase zone. The Nu can be calculated by Eq. (25):

$$Nu=\xi Nu_{An}+(1-\xi)Nu_{Ls} \tag{25}$$

where the ξ is calculated by Eq. (26):

$$\xi=\frac{\chi}{\chi+(1-\chi)\rho_V/\rho_L} \tag{26}$$

The Nu_{An} is calculated by Eq. (27):

$$Nu_{An}=\left(Nu_{An,F}^3+Nu_{An,S}^3\right)^{1/3} \tag{27}$$

The $Nu_{An,F}$ is calculated by Eq. (28):

$$Nu_{An,F}=\frac{\varphi}{1-\chi}\sqrt{f_{Vo}\frac{\rho_L}{\rho_V}}Re_L^{0.5}\left(0.6+0.06+Re_L^{0.4}Pr_L^{0.3}\right) \tag{28}$$

The $Nu_{An,S}$ is calculated by Eq. (29):

$$Nu_{An,S}=0.51\left[\frac{\rho_L\Delta h_{LV}\sigma_{fi}d}{u_L\lambda_L(T_s-T_w)}\right]^{0.25} \tag{29}$$

The Φ_{Vo} is calculated by Eq. (30):

$$\varphi_{Vo}=\sqrt{\chi^{1.8}+(1-\chi)^{1.8}\frac{\rho_V f_{Lo}}{\rho_L f_{Vo}}+0.65\chi^{0.68}(1-\chi)^{1.43}\left(\frac{u_L}{u_V}\right)^{1.25}\left(\frac{\rho_V}{\rho_L}\right)^{0.75}} \tag{30}$$

The Nu_{Ls} is calculated by Eq. (31):

$$Nu_{Ls}=\begin{cases}\dfrac{(f_L/2)(Re_L-1000)Pr_L}{1+12.7\sqrt{f_L/2}\left(Pr_L^{2/3}-1\right)} & \text{for } Re_L\geq 2000\\ 8.23\left(1-1.891a^*+2.22a^{*2}-0.894a^{*3}\right) & \text{for } Re_L<2000\end{cases} \tag{31}$$

Therefore, the heat transfer of refrigerant in each small element can be expressed as Eq. (32):

$$Q_{con,i}=\left(t_{r,i}-t_w\right)\Big/\left[\frac{1}{L_i}\left(\frac{1}{h_{r,i}(240\sigma_{cm}+480HF)}+\frac{\delta_{cm}}{20y\lambda_{cm}}+\frac{\delta_{tk}Af_{tk}}{20y\lambda_{tk}}+\frac{Af_{tk}}{20yh_{w,i}}\right)+R\right] \tag{32}$$

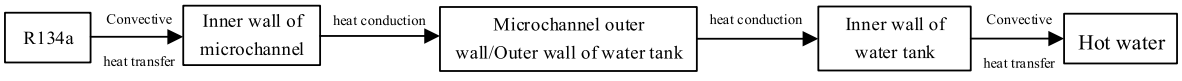

Fig. 10. Heat transfer process from refrigerant to the water in the storage tank.

Then the heat transfer of refrigerant in the condenser, namely the heat gain of the hot water storage tank, can be obtained from Eq. (33):

$$Q_{con} = \sum_{i=1}^{n} Q_{con,i} \tag{33}$$

3.3. Electronic expansion valve model

The high-pressure subcooled refrigerant enters the electronic expansion valve and then expands. This process can be regarded as an isenthalpic expansion, as Eq. (34) shows:

$$h_{eev,in,i} = h_{eev,out,i} \tag{34}$$

3.4. System model and working conditions

The components selected for the system and the parameters used in the modeling and simulation are listed in Tables 1 and 2

The operation performance of the uninsulated micro-channel PV/T heat pump water heater (UMC-PVT-HPWH) system is mainly affected by ambient temperature, solar radiation intensity and wind speed [36], which are analyzed under different working conditions. In the simulation, the initial water temperature of the storage tank, the termination temperature for heating, and the volume of the storage tank are set as the initial parameters for program execution. Their values are determined according to GB/T 23889-2009 [37] as 20 °C, 60 °C, and 100 L, respectively. The basic working conditions are selected based on the average values for the parameters of winter in Beijing in typical meteorological years, referring to the Chinese building thermal environment analysis of specialized meteorological data collection. The solar radiation intensity of basic working conditions is 322 W/m^2, the ambient temperature is 12.6 °C, and the wind speed is 2.4 m/s. Based on the basic working conditions, the performance of the system under different solar radiant intensity, ambient temperature and wind speed is simulated, the ranges of which are 0–1000 W/m^2, -18.6–32.6 °C and 0.4–4.4 m/s, respectively. The specific working condition parameters are shown in Table 3. The outlet superheat degree of the UMC-PVT-SC and the outlet subcooled degree of micro-channel condenser are both set at 5 °C, and the time step is 1 min. The flow chart of the system modeling and simulation is given in Fig. 12.

3.5. Performance indicators

The collector efficiency of the UMC-PVT-SC is equal to the ratio of the heat obtained by the UMC-PVT-SC to the incident solar energy on the PV panel surface, which can be calculated by Eq. (35):

Table 3
Key weather parameters and simulation conditions.

Key weather parameters	*Solar radiation intensity* I *(W/m^2)*	*Ambient temperature* t_a *(°C)*	*Wind speed* u_w *(m/s)*	*Water temperature* t_w *(°C)*
Solar radiation	0/122/222/322/422/522/622/722/822/922/1000	12.6	2.4	20–60
Ambient temperature	322	−18.6/-8.6/2.6/12.6/22.6/32.6	2.4	20–60
Wind speed	322	12.6	0.4/1.4/2.4/3.4/4.4	20–60

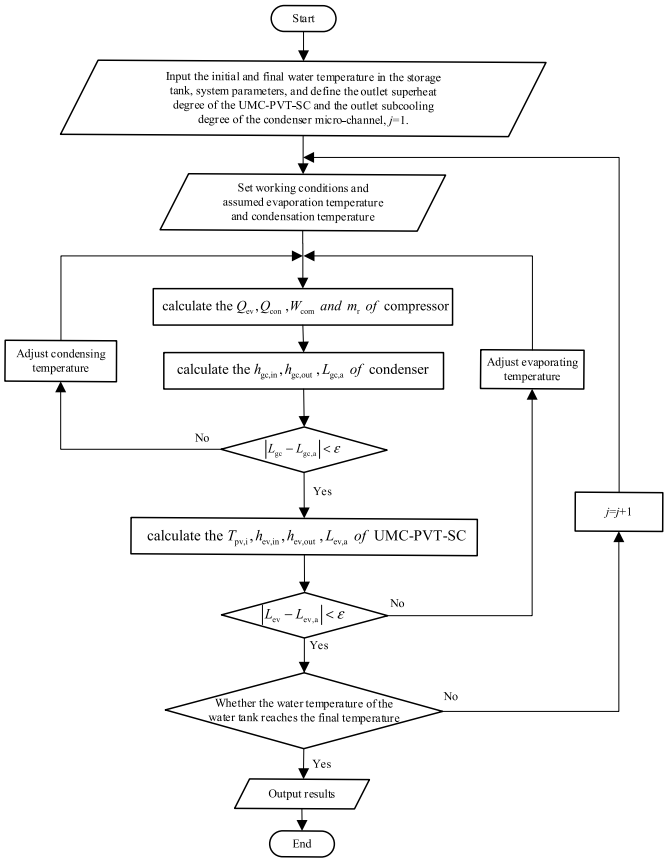

Fig. 12. Flow chart of the system modeling and simulation.

$$\eta_t = \frac{\sum_{j=1}^{z} Q_{ev,j}}{\sum_{j=1}^{z} A_{pvt} I_j} \tag{35}$$

The electric efficiency of the UMC-PVT-SC is equal to the ratio of the power generated by the photovoltaic cell to the incident solar energy on the surface of the PV cell, which can be calculated by Eq. (36):

$$\eta_e = \frac{\sum_{j=1}^{z} E_j}{\sum_{j=1}^{z} A_{pv} I_j} \tag{36}$$

In this study, the UMC-PVT-SC provides both thermal and electrical energies, and in some operating conditions, its power generation may exceed the power consumption of the system (compressor), resulting in unreasonable evaluation of the overall energy utilization efficiency of the system. The photovoltaic power generation should be evaluated by the converted equivalent thermal energy. The overall efficiency of the UMC-PVT-SC can be expressed as Eq. (37) [38]:

$$\eta_{pvt} = \frac{A_{pv}\eta_e}{0.38 A_{pvt}} + \eta_t \tag{37}$$

The *COP* of a conventional heat pump is defined as the ratio of the heat provision to the power consumed by the compressor, calculated by Eq. (38):

$$COP_{HP} = \frac{\sum_{j=1}^{z} Q_{con,j}}{\sum_{j=1}^{z} W_{com,j}} \tag{38}$$

The overall coefficient of performance of the UMC-PVT-HPWH system is defined by Eq. (39) [38]:

$$COP_{\mathrm{pvt}} = \frac{\sum_{j=1}^{z} Q_{\mathrm{con,j}} + \sum_{j=1}^{z} E_{\mathrm{j}} \Big/ 0.38}{\sum_{j=1}^{z} W_{\mathrm{com,j}}} \tag{39}$$

The UMC-PVT-SC is the core component of the system. It is very important to analyze the heat sources of the collector and the ratio of solar energy and air source. These two heat sources are defined as follows:

The total incident solar energy on the PV panel surface can be calculated by Eq. (40):

$$Q_{\mathrm{inc}} = IA_{\mathrm{pvt}} \tag{40}$$

The thermal energy absorption by PV panel can be calculated by Eq. (41):

$$Q_{\mathrm{pv}} = \sum_{\mathrm{i}=1}^{\mathrm{n}} Q_{\mathrm{pv,i}} \tag{41}$$

The thermal energy absorption by convection from the bottom surface of micro-channel tubes of the micro-channel evaporator can be calculated by Eq. (42):

$$Q_{\mathrm{b}} = \sum_{i=1}^{n} Q_{b,i} \tag{42}$$

The thermal energy absorption of PV panel by convection can be calculated by Eq. (43):

$$Q_{\mathrm{convpv}} = h\sum_{\mathrm{i}=1}^{\mathrm{n}} A_{\mathrm{pvt,i}}\left(t_{\mathrm{a}} - t_{\mathrm{pv,i}}\right) + 12hH\sum_{\mathrm{i}=1}^{\mathrm{n}} L_{\mathrm{i}}\left(t_{\mathrm{a}} - t_{\mathrm{pv,i}}\right) \tag{43}$$

The thermal energy absorption of the UMC-PVT-SC by convection can be defined by Eq. (44):

$$Q_{\mathrm{conv}} = Q_{\mathrm{b}} + Q_{\mathrm{convpv}} \tag{44}$$

The thermal energy absorption of PV panel by radiation can be expressed as Eq. (45):

$$Q_{\mathrm{rad}} = \sum_{\mathrm{i}=1}^{\mathrm{n}} Q_{\mathrm{rad,i}} \tag{45}$$

The total thermal energy absorption of photothermal conversion of the UMC-PVT-SC can be expressed as Eq. (46):

$$Q_{\mathrm{pt}} = Q_{\mathrm{ev}} - Q_{\mathrm{conv}} - Q_{\mathrm{rad}} \tag{46}$$

4. Experimental verification and result analysis

4.1. Validation of the mathematical model

The experimental platform for the proposed system is built in Beijing. Experiments under real outdoor weather conditions are conducted for over 30 days in summer and winter. Typical data from one testing day (Fig. 13) are selected as input parameters for comparisons between the experimental data and simulation results. The system is simulated based on the weather conditions of the testing day.

As is seen from Fig. 14, the evaporation temperature and PV panel temperature increase as the solar radiation intensity and ambient temperature increase. The simulation results of evaporation temperature, PV panel temperature, condensation temperature and water temperature in the water tank agree well with the experimental data, within 8.3 %, 10.5 %, 2.7 % and 3.4 %, respectively. This suggests that the assumption of neglecting the contact thermal resistance is acceptable although actually there is certain contact thermal resistance between the micro-channel tubes and the backplane of the PV panel due to imperfect bonding during the integrated processing of PV/T modules.

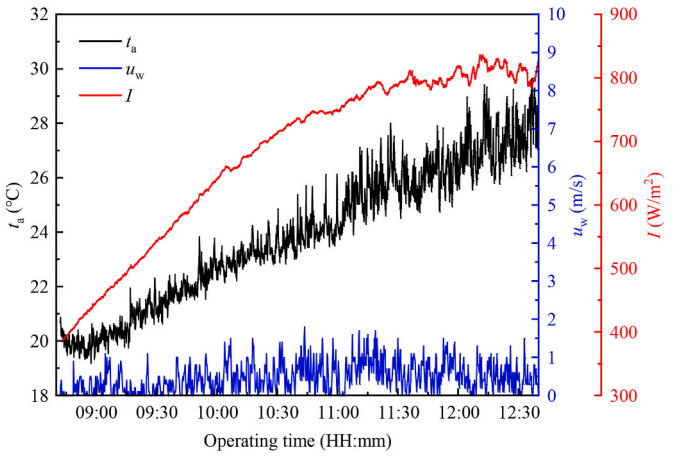

Fig. 13. Variation of solar irradiance, ambient temperature and wind speed during the testing day.

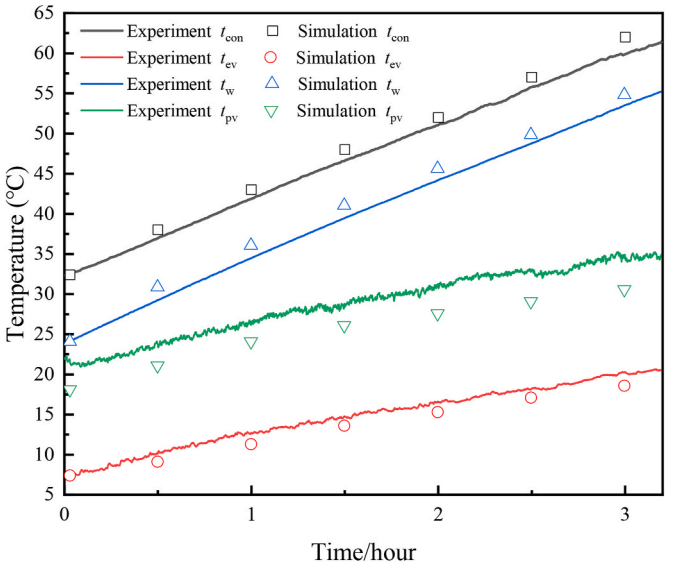

Fig. 14. Comparison of the simulated temperatures with experimental data.

As is seen from Fig. 15, the averaged differences between the simulation results and experimental data of the compressor power consumption and PV power generation are 4.4 % and 8.1 %, respectively, while the maximum differences of the heat gains of condenser and UMC-PVT-SC are 11.5 % and 7.1 %, respectively. In terms of the heat gain of the system, the simulated value is higher than the experimental one because, in the simulation, the overall thermal resistance between the refrigerant and PV panel is smaller. Therefore, the system absorbs more heat in the simulation.

As can be seen from Fig. 16, the COP_{HP} and COP_{pvt} decrease with the system operation time. The averaged differences between the numerical results and experimental data are 9.6 % and 12 %, respectively. As can be seen from Fig. 17, the efficiency decreases with the system operation time. The averaged differences of the collector efficiency, electrical efficiency and total efficiency are 8.3 %, 8.1 % and 3.2 %, respectively. The simulation results and experimental data are compared and analyzed for the temperature, heat transfer rate, compressor power consumption, PV power generation and *COP*. The comparison results show that all the differences are less than 15 %, which verifies the accuracy of the models developed in the present work.

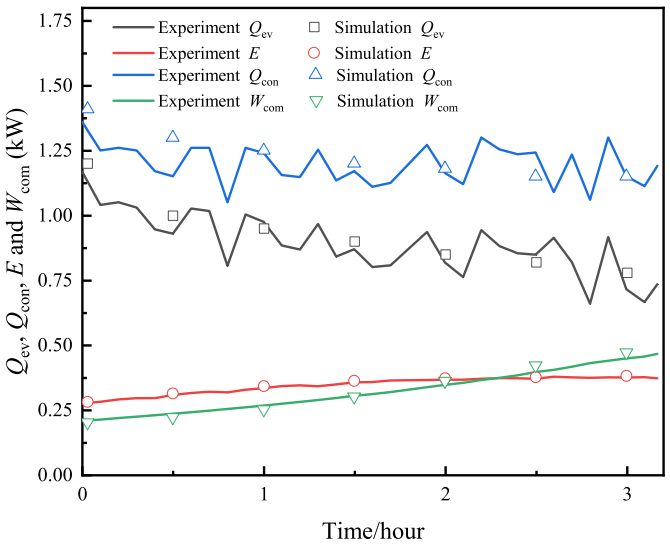

Fig. 15. Comparison of the simulated results with experimental data for heat gains of condenser and UMC-PVT-SC, compressor power consumption and PV power generation.

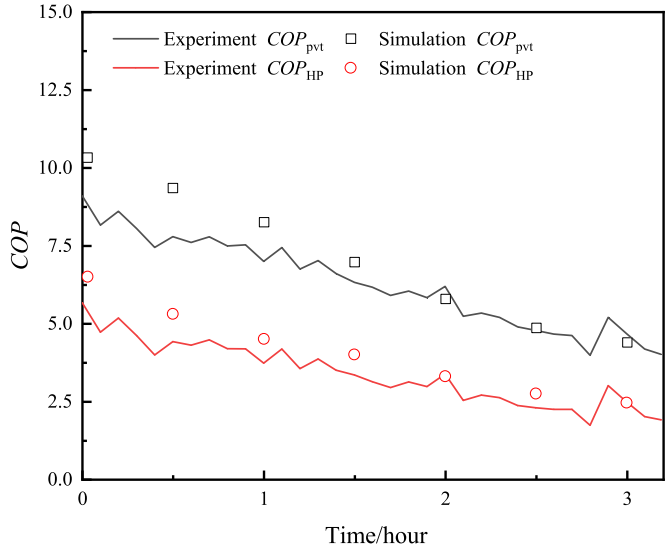

Fig. 16. Comparison of the simulated *COP*s with experimental ones.

4.2. Influence of solar radiation intensity on system operation performance

For this condition, the ambient temperature and wind speed are set at 12.6 °C and 2.4 m/s, and the solar radiation intensity changes from 0 W/m^2 to 1000 W/m^2. As shown in Fig. 18, as solar radiation intensity increases from 0 W/m^2 to 1000 W/m^2, the PV cell temperature, evaporation temperature, evaporation pressure and mass flow rate of refrigerant increase gradually, while the condensation temperature and pressure merely change. The PV cell temperature increases from 3.96 °C to 17.24 °C. The evaporation pressure increases from 277.60 kPa to 353.57 kPa. The evaporation temperature increases from −1.57 °C to 5.29 °C. Mass flow rate increases from 0.0072 kg/s to 0.00916 kg/s. The condensation temperature ranges from 46.12 °C to 47.10 °C. The condensation pressure ranges from 1223.00 kPa to 1259.37 kPa. The reason is that the evaporator of the system absorbs thermal energy in two ways: one is from ambient air, and the other is the heat converted by the PV cell from the solar radiation. When the solar radiation intensity increases, the thermal energy from photothermal conversion increases,

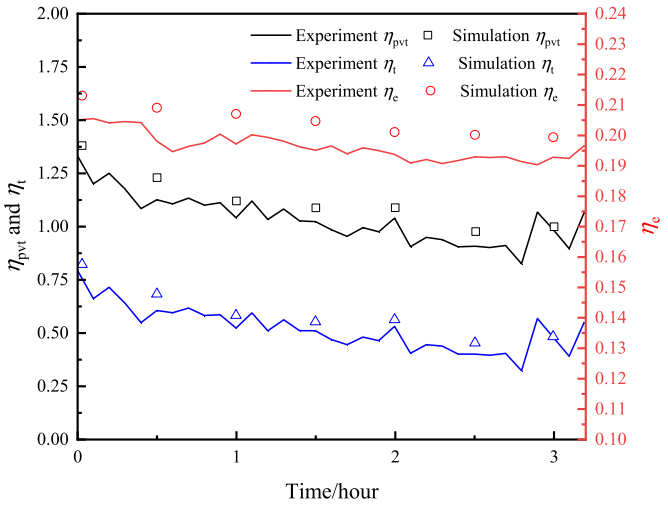

Fig. 17. Comparison of the simulated efficiencies with experimental ones.

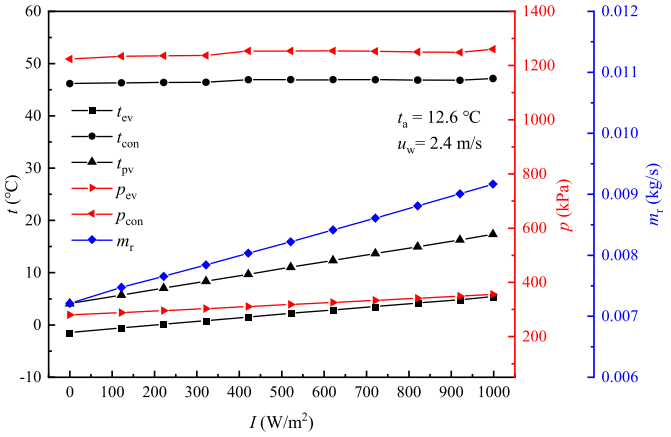

Fig. 18. Evaporation temperature and pressure, condensation temperature and pressure and refrigerant mass flow rate vs solar radiation intensity.

and the refrigerant temperature in the UMC-PVT-SC rises, which improves the evaporation temperature and pressure. As a result, the suction pressure of the compressor increases, the pressure ratio decreases, and the mass flow rate of the refrigerant increases. To maintain the temperature difference of heat transfer, the temperature of PV cell rises synchronously. In this condition, the temperature of water does not change much, so the parameters of condensation process do not change much.

As shown in Fig. 19, with the increase of solar radiation intensity from 0 W/m^2 to 1000 W/m^2, the thermal energy absorption of the UMC-PVT-SC decreases significantly from 1106.6 W to −20.5 W. The thermal energy absorption from the bottom by convection of the micro-channel tube decreases from 547.9 W to 283 W. The thermal energy absorption by convection of PV panel decreases from 558.7 W to −303.4 W. The radiation heat dissipation of PV panel increases from 88.4 W to 219.7 W. The thermal energy absorption by photothermal conversion of the UMC-PVT-SC increases from 0 W to 1550.8 W. The thermal energy absorption from PV panel increases from 470.3 W to 1027.7 W. As is seen from Fig. 18 that as solar radiation intensity increases, at first, the PV panel temperature is lower than the ambient temperature; when the solar radiation intensity reaches 722 W/m^2, the PV panel temperature starts to be higher than the ambient temperature. At that time, the PV panel starts to lose heat to the surrounding environment. During the whole process, the PV panel temperature is always higher than the effective sky temperature, thus the PV panel always emits thermal energy into the

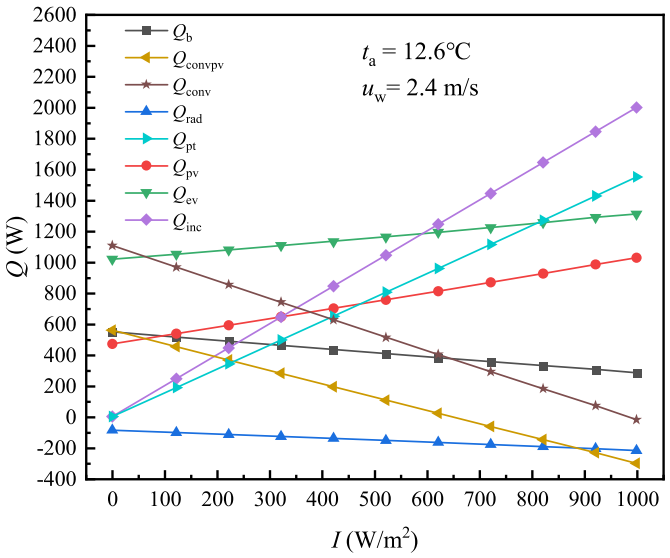

Fig. 19. Total solar radiation, heat gain of UMC-PVT-SC and heat sources of UMC-PVT-SC vs solar radiation intensity.

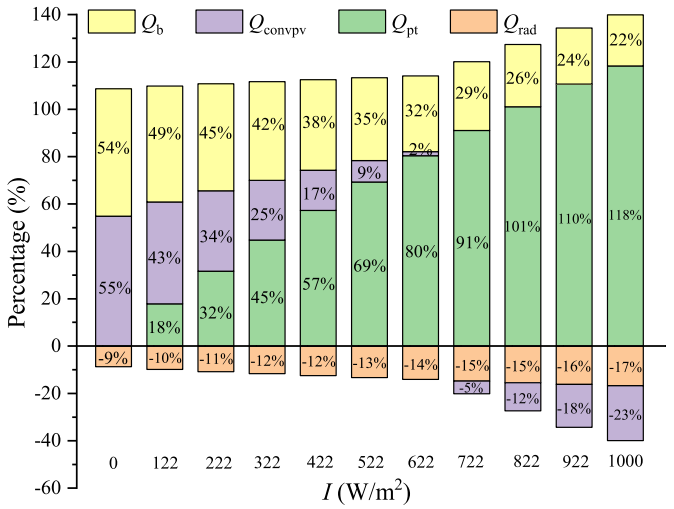

Fig. 21. Contribution rate of each heat source to heat gain of evaporator vs solar radiation intensity.

sky. Therefore, when solar radiation intensity is 0 W/m^2, the thermal energy absorption of PV panel by convection. As can be seen from Figs. 20 and 21 that as solar radiation intensity increases, the ratio of each heat source in the heat gain of the UMC-PVT-SC changes regularly. During the whole process, the heat gains of the UMC-PVT-SC are from the thermal absorption by convection and photothermal conversion. When solar radiation intensity is 122 W/m^2, the UMC-PVT-SC mainly absorbs heat by convective heat transfer, which accounts for 92 % of the total heat gain. The thermal energy absorption by photothermal conversion of the UMC-PVT-SC accounts for 18 %, while the thermal energy absorption by radiation of PV panel accounts for only −10 %. With the increase of solar radiation intensity, the thermal energy absorption by photothermal conversion of the UMC-PVT-SC increases and plays a leading role gradually. When solar radiation intensity reaches 1000 W/m^2, the thermal energy absorption by photothermal conversion of the UMC-PVT-SC accounts for 118 % of the total heat gain. The thermal energy absorption by convection of the UMC-PVT-SC accounts for −1%, and the thermal energy absorption by radiation of PV panel accounts for −17 %. As the main heat source for UMC-PVT-SC, the thermal energy absorption by photothermal conversion is mainly affected by solar radiation intensity. Therefore, with the increase of solar radiation intensity, the thermal energy absorption by photothermal conversion of the UMC-PVT-SC increases synchronously, which leads to the increase of the temperature of PV panel, and the decrease of the convection thermal energy absorption of the UMC-PVT-SC. As the temperature of the PV cell rises, the temperature difference between the PV cell and the effective sky temperature increases, thus the radiation heat dissipation of PV panel increases.

As shown in Fig. 22, with the increase of solar radiation intensity from 0 W/m^2 to 1000 W/m^2, the heat gain of condenser, PV power generation and heat gain of the UMC-PVT-SC increase significantly. The power consumption of compressor increases slowly. The system pressure ratio decreases gradually. The heat transfer of condenser to water increases from 1269.0 W to 1579.6 W. The heat gain of the UMC-PVT-SC almost linearly increases from 1018.2 W to 1310.7 W. The compressor power consumption increases from 250.8 W to 268.9 W. The electricity generation increases from 0 W to 409.6 W. The pressure ratio decreases from 4.40 to 3.52. As evaporation temperature increases, the temperature difference for heat transfer at the evaporation side decreases and the temperature difference between the PV panel and effective sky increases. Therefore, the thermal energy absorption by convection of the

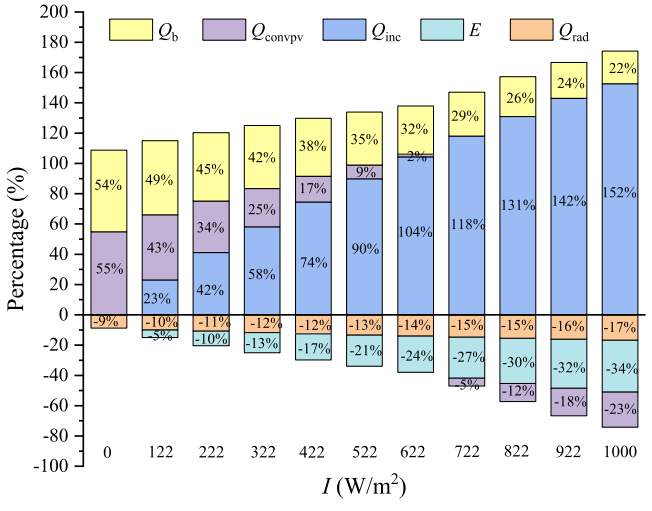

Fig. 20. Contribution rate of each heat source to heat gain of UMC-PVT-SC vs solar radiation intensity.

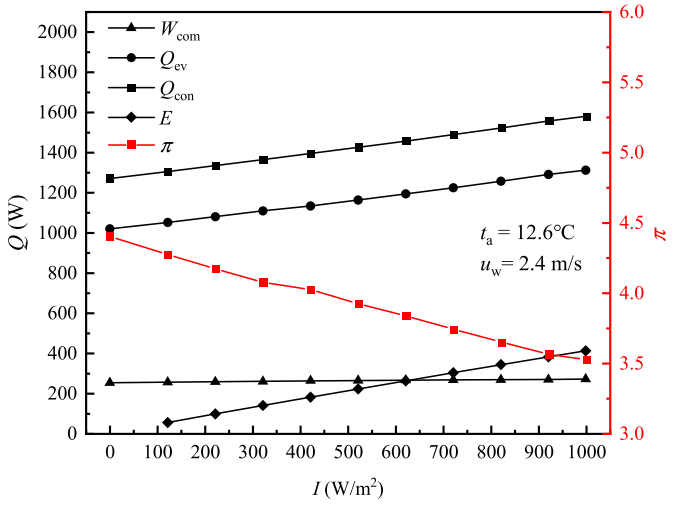

Fig. 22. PV power generation, heat gain of condenser, heat gain of UMC-PVT-SC, compressor power consumption and pressure ratio vs solar radiation intensity.

UMC-PVT-SC reduces and the radiation heat dissipation of PV panel gradually increases, but the sum of the decrease of the convection thermal energy absorption and the increase of the radiation heat dissipation is less than the thermal energy absorption by photothermal conversion of the UMC-PVT-SC. Therefore, with the increase of the solar radiation intensity, the heat gain of the UMC-PVT-SC still shows an increasing trend, the system pressure ratio decreases gradually, and the enthalpy difference between the inlet and outlet of the compressor decreases. However, the mass flow rate of refrigerant increases gradually, where the increasing trend is larger than the decreasing trend of the enthalpy difference between the inlet and outlet of the compressor. Therefore, the power consumption of the compressor increases gradually in a small variation range. With the increase of solar radiation intensity, the evaporation pressure increases, the system pressure ratio decreases, and the heating capacity increases. The heat gain of the UMC-PVT-SC increases. The power generation of PV cell is mainly affected by solar radiation intensity.

As shown in Fig. 23, with the increase of solar radiation intensity from 0 W/m^2 to 1000 W/m^2, The COP_{HP} and COP_{pvt} increase. The water heating time decreases. The collector efficiency and overall energy efficiency of the UMC-PVT-SC decrease significantly at first and then decrease gradually, while the electric efficiency decreases gradually in a small range. COP_{HP} increases almost linearly from 5.36 to 6.17. COP_{pvt} increases almost linearly from 5.92 to 10.35. The collector efficiency of the UMC-PVT-SC decreases from 4.31 to 0.66. The overall energy efficiency decreases from 4.87 to 1.19. The heating time decreases from 218.04 min to 175.11 min. The electric efficiency of the UMC-PVT-SC decreases from 0.222 to 0.211. The energy of photothermal conversion, as the main heat source for UMC-PVT-SC, increases almost linearly as solar radiation intensity increases, whose ratio gradually increases. Therefore, with the increase of solar radiation intensity, the heat gains of the UMC-PVT-SC and condenser increases. Since the increase of compressor power consumption is smaller than the increase of heat gain of condenser, COP_{HP}, COP_{pvt} and the heating capacity of the system increase while the heating time decreases. As the solar radiation intensity increases, the surface temperature of the UMC-PVT-SC increases, the convection heat transfer temperature difference decreases, and the heat obtained by the refrigerant from the ambient air decreases. The increase in the amount of heat absorbed by the evaporator is smaller than the increase in the total amount of solar radiation received. Therefore, the collector efficiency of the UMC-PVT-SC sharply decreases at first and then decreases gradually. With the increase of solar radiation intensity, the temperature of PV cell increases. As the electric efficiency of the UMC-PVT-SC is mainly affected by the temperature of PV cell, it gradually decreases. The overall energy efficiency of the UMC-PVT-SC is mainly related to the collector efficiency Thus, the overall efficiency and the collector efficiency of the UMC-PVT-SC show the same variation trend.

4.3. Influence of ambient temperature on system operation performance

For this condition, the solar radiation intensity and wind speed are set at 322 W/m^2 and 2.4 m/s, respectively, and the ambient temperature changes from −18.6 °C to 32.6 °C. As shown in Fig. 24, with the increase of ambient temperature from −18.6 °C to 32.6 °C, the PV cell temperature, evaporation temperature and evaporation pressure increase almost linearly. The mass flow rate of refrigerant also increases. The condensation temperature and condensation pressure are not greatly affected by the ambient temperature. The temperature of PV cell increases from −18.75 °C to 24.64 °C. The evaporation temperature increases from −22.61 °C to 13.31 °C. The evaporation pressure increases from 118.47 kPa to 462.97 kPa. The mass flow rate increases from 0.00356 kg/s to 0.01188 kg/s. The condensation temperature ranges from 44.44 °C to 48.00 °C. The condensation pressure ranges from 1179.20 kPa to 1287.00 kPa. When the ambient temperature increases, the temperature difference between the refrigerant at the evaporating side and the ambient air increases, and the temperature difference between the PV panel and effective sky temperature decreases, thus the convection thermal energy absorption of the UMC-PVT-SC increases, and the radiation heat dissipation of PV panel decreases. The heat exchange at the evaporator side is enhanced and the temperature of the refrigerant in the UMC-PVT-SC increases. Thereby the evaporation temperature and evaporation pressure are increased. The compressor suction pressure increases, the pressure ratio decreases, and the refrigerant mass flow rate increases. Under this condition, the water temperature is merely changed and thus the parameters at the condensing side are merely changed.

As shown in Fig. 25, with the increase of ambient temperature from −18.6 °C to 32.6 °C, the thermal energy absorption by convection of the UMC-PVT-SC increases from 162.2 W to 1261.4 W. The thermal energy absorption by convection from the bottom of the micro-channel increases from 152.6 W to 751.9 W. The thermal energy absorption by convection of PV panel increases from 9.7 W to 509.5 W. The thermal energy dissipation by radiation of PV panel increases from 180.9 W to 24.9 W. The thermal energy absorption by photothermal conversion of the UMC-PVT-SC ranges from 481.0 W to 503.1 W. The thermal energy absorption from PV panel increases from 309.8 W to 988.1 W. As can be seen from Figs. 26 and 27 that as ambient temperature increases, the ratio of each heat source in the heat gain of the UMC-PVT-SC changes regularly. During the whole process, the heat gain of the UMC-PVT-SC is composed of the thermal energy absorption by convection and photothermal conversion. When ambient temperature is −18.6 °C, the UMC-PVT-SC mainly absorbs heat by photothermal conversion, which

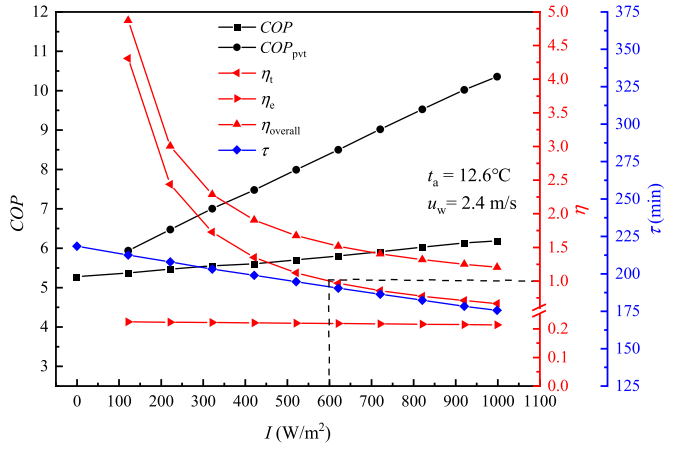

Fig. 23. Collector efficiency, electric efficiency and overall energy efficiency of the UMC-PVT-SC, heating time, *COP* and COP_{pvt} vs solar radiation intensity.

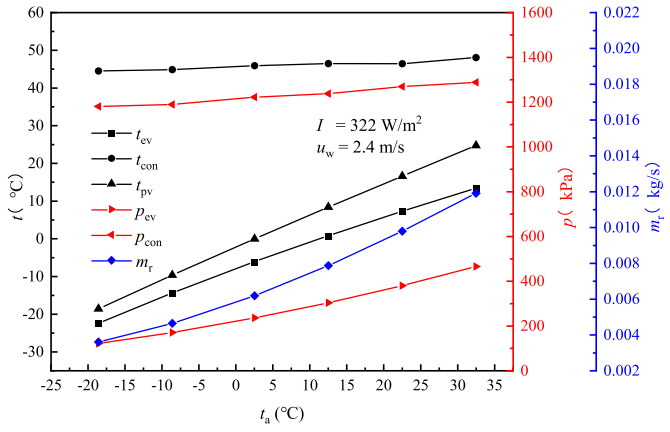

Fig. 24. Evaporation temperature and pressure, condensation temperature and pressure, and refrigerant mass flow rate vs ambient temperature.

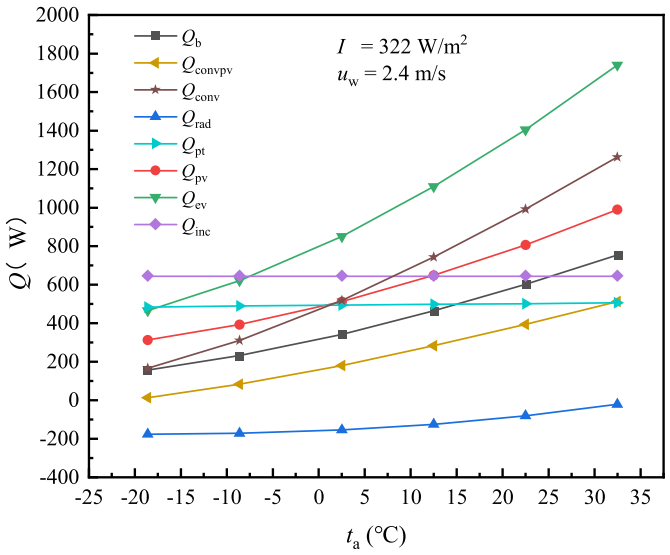

Fig. 25. Total solar radiation, heat gain of UMC-PVT-SC and heat sources of UMC-PVT-SC vs ambient temperature.

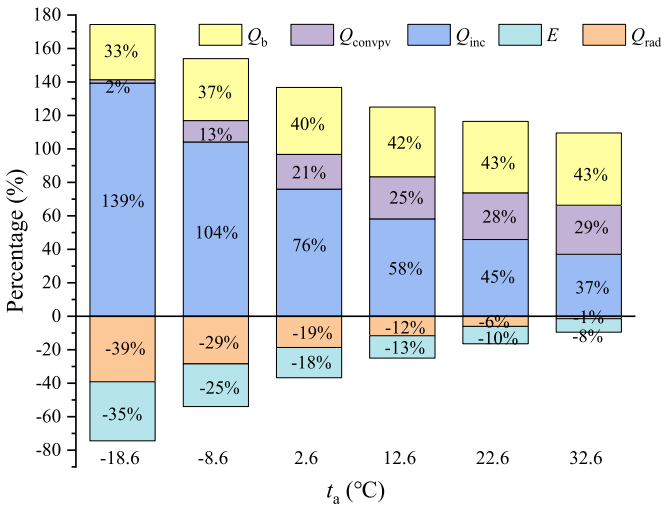

Fig. 26. Contribution rate of each heat source to heat gain of UMC-PVT-SC vs ambient temperature.

accounts for 104 % of the total heat gain. The convection heat absorption of the UMC-PVT-SC accounts for 35 %, while the radiation heat absorption of PV panel accounts for −39 %. When ambient temperature reaches 32.6 °C, the thermal energy absorption by photothermal conversion of the UMC-PVT-SC accounts for 29 % of the total heat gain. The thermal energy absorption by convection of the UMC-PVT-SC accounts for 72 %, and the radiation heat absorption of PV panel accounts for −1%. This is mainly caused by the increase of evaporation temperature, but the increase is smaller than the increase of ambient temperature. The temperature difference of convection heat transfer gradually increases, so the thermal energy absorption by convection of the UMC-PVT-SC increases. The temperature of PV cell increases as ambient temperature rises but the magnitude of the increase in PV cell temperature is smaller than that of the increase in effective sky temperature. The temperature difference between the PV cell and effective sky temperature decreases, and thus the PV cell emits less thermal energy to the sky. As solar radiation intensity remains at the given value, the thermal energy absorption by photothermal conversion of the UMC-PVT-SC basically remains unchanged.

As shown in Fig. 28, with the increase of ambient temperature from

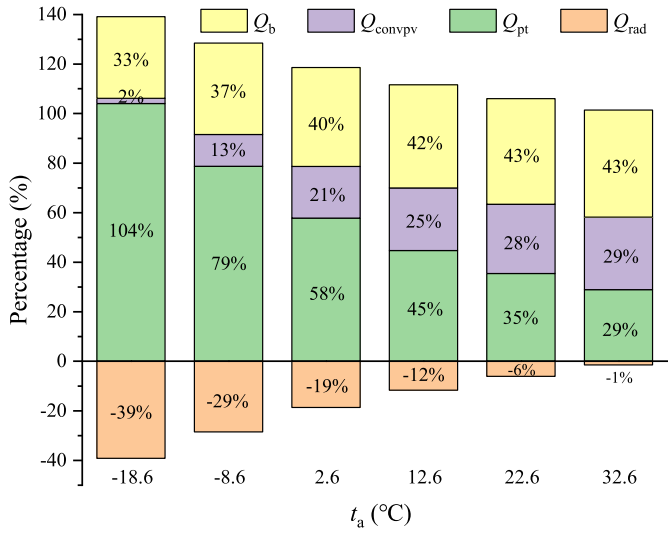

Fig. 27. Contribution rate of each heat source to heat gain of evaporator vs ambient temperature.

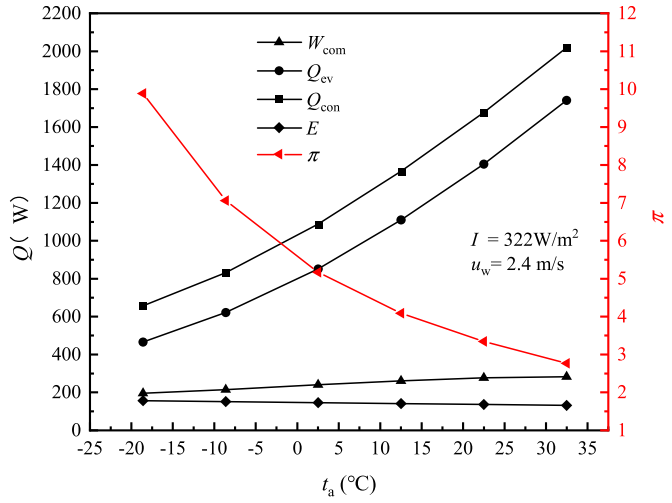

Fig. 28. Power generation, heat gain of condenser, heat gain of UMC-PVT-SC, compressor power consumption and pressure ratio vs ambient temperature.

−18.6 °C to 32.6 °C, the heat gains of the condenser and UMC-PVT-SC increases significantly. The power consumption of compressor increases slowly. The system pressure ratio decreases. The PV power generation basically decreases slowly. The heat transfer of condenser increases from 654.0 W to 2018.7 W. The thermal energy absorption of evaporator increases from 462.3 W to 1740.0 W. The compressor power consumption increases from 191.6 W to 278.7 W. The pressure ratio decreases from 9.88 to 2.75. The PV power generation is maintained between 152.5 W and 127.6 W. As ambient temperature increases, the evaporation temperature increases, the temperature difference for heat transfer at the evaporation side increases. The convective heat transfer between the UMC-PVT-SC and the ambient air increases gradually, the radiation heat dissipation of PV panel decreases, and the energy of photothermal conversion absorbed by the UMC-PVT-SC basically remains unchanged. Therefore, the heat absorbed by the evaporator shows an increasing trend. As ambient temperature increases, the system pressure ratio decreases, and the enthalpy difference between the inlet and outlet of the compressor decreases. The refrigerant mass flow rate gradually increases, whose increasing trend is larger than the decreasing trend of the enthalpy difference between the compressor inlet and outlet. Thus, the power consumption of the compressor gradually

increases in a small range. As ambient temperature increases, the evaporation pressure increases, the system pressure ratio decreases, and the heating capacity increases. At the same time, the increase of mass flow rate also improves the heat exchange capacity in the heat exchange processes. The thermal energy absorption of the UMC-PVT-SC increases, and the heat exchange of the condenser increases simultaneously. The power generation of PV cell gradually decreases due to the temperature rise of the PV panel.

As shown in Fig. 29, with the increase of ambient temperature from −18.6 °C to 32.6 °C, The collector efficiency and overall energy efficiency of UMC-PVT-SC increase. COP_{HP} and COP_{pvt} increase. The water heating time decreases significantly. The electric efficiency of the UMC-PVT-SC gradually decreases in a small range. COP_{HP} increases from 3.50 to 7.73. COP_{pvt} increases from 5.63 to 9.00. The collector efficiency of the UMC-PVT-SC increases from 0.718 to 2.702. The overall energy efficiency of the UMC-PVT-SC increases from 1.341 to 3.220. The water heating time decreases from 422.07 min to 137.00 min. The electric efficiency of UMC-PVT-SC decreases from 0.2442 to 0.2109. With the increase of ambient temperature, the heat gains of the UMC-PVT-SC and condenser increases. Since the increase in the power consumption of the compressor is smaller than the increase in the heat gain of condenser, COP_{HP} and COP_{pvt} increase, the heating capacity of the system increases, and the water heating time decreases. As ambient temperature rises, the temperature of PV cell rises synchronously. Since the electric efficiency is mainly affected by the temperature of PV cell, the electric efficiency gradually decreases. With the increase of ambient temperature, the heat gain of the UMC-PT-SC increases, while the total amount of solar radiation received on the surface of the solar collector remains unchanged. Therefore, the collector efficiency of UMC-PVT-SC gradually increases, and the overall energy efficiency of the system also increases synchronously.

4.4. Influence of wind speed on system operation performance

Wind speed affects the heat gain of the UMC-PVT-SC by changing the convective heat transfer coefficient on the surface, and then affects the performance of the system. Among meteorological parameters, compared with ambient temperature and solar radiation intensity, wind speed has less influence on the performance of heat pump system. In this paper, solar radiation intensity and ambient temperature are set at 322 W/m^2 and 12.6 °C, respectively, and wind speed changes from 0.4 m/s to 4.4 m/s, the temperature of the PV panel is always lower than the ambient temperature, and the refrigerant absorbs heat from the ambient air through convection heat transfer.

As shown in Fig. 30, with the increase of wind speed from 0.4 m/s to 4.4 m/s, the PV cell temperature, evaporation temperature and

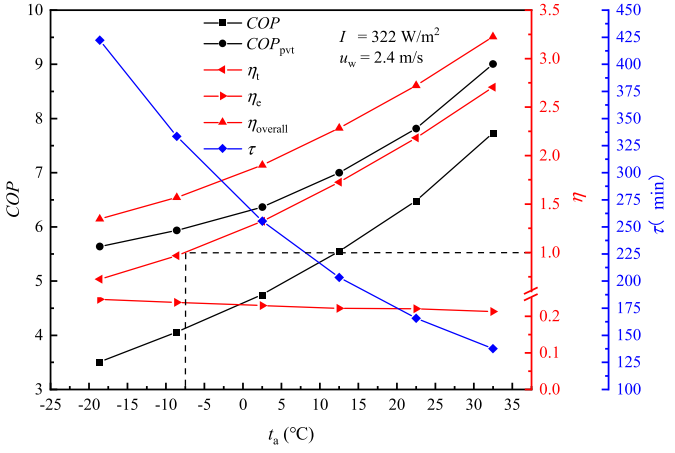

Fig. 29. Collector efficiency, electric efficiency and overall energy efficiency of the UMC-PVT-SC, heating time, *COP* and COP_{pvt} vs ambient temperature.

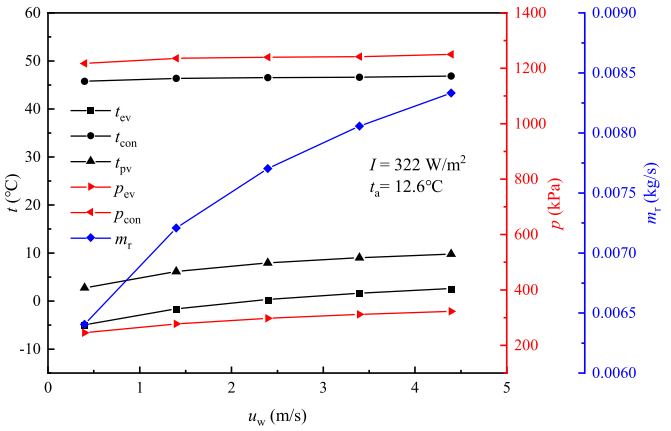

Fig. 30. Evaporation temperature and pressure, condensation temperature and pressure and refrigerant mass flow rate vs wind speed.

evaporation pressure rise slightly. The refrigerant mass flow rate rises significantly. The condensation temperature and condensation pressure merely change. The PV cell temperature increases from 2.63 °C to 9.66 °C. The evaporation temperature increases from −5.11 °C to 2.47 °C. The evaporation pressure increases from 242.75 kPa to 320.15 kPa. The refrigerant mass flow rate increases from 0.0064 kg/s to 0.00833 kg/s. The condensation temperature ranges from 45.7 °C to 46.8 °C. The condensation pressure ranges from 1216.61 kPa to 1249.30 kPa. The increase in wind speed leads to the increase in overall heat transfer coefficient of the evaporator between the refrigerant and the ambient air sides, which enhances the thermal energy absorption between the UMC-PVT-SC and the ambient air by convection. Therefore, the evaporation temperature and pressure increase, the suction pressure of the compressor increases, and the pressure ratio decreases, leading to an increase of the refrigerant mass flow rate. Under this condition, the water temperature merely changes, thus the parameters at the condensing side merely change.

As shown in Fig. 31, with the increase of wind speed from 0.4 m/s to 4.4 m/s, the thermal energy absorption by convection of the UMC-PVT-SC increases from 474.2 W to 828.7 W. The thermal energy absorption by photothermal conversion of the UMC-PVT-SC basically remains unchanged. The thermal energy absorption by convection of PV panel increases from 235.0 W to 280.2 W, and then gradually decreases to

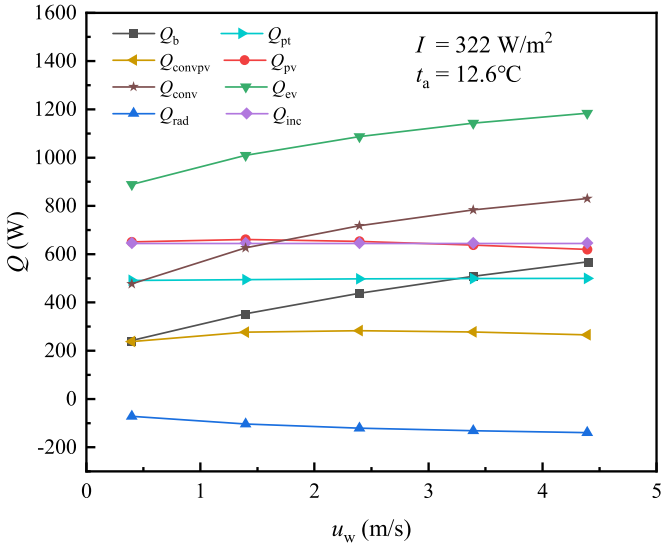

Fig. 31. Total solar radiation, heat gain of UMC-PVT-SC and heat sources of UMC-PVT-SC vs wind speed.

263.04 W. The thermal energy absorption from PV panel increases from 648.1 W to 658.4 W, and then gradually decreases to 617.0 W. The radiation heat dissipation of PV panel increases from 75.8 W to 142.9 W. The thermal energy absorption by photothermal conversion of the UMC-PVT-SC ranges from 489.0 W to 496.8 W. As can be seen from Figs. 32 and 33 that as wind speed increases, the ratio of each heat source in the heat gain of the UMC-PVT-SC changes regularly. When wind speed is 0.4 m/s, the thermal energy absorption by photothermal conversion of the UMC-PVT-SC accounts for 55 % of the total heat gain. The thermal energy absorption by convection of the UMC-PVT-SC accounts for 53 %, while the thermal energy absorption by radiation of PV panel accounts for −8%. With the increase of wind speed, the thermal energy absorption by photothermal conversion of the UMC-PVT-SC basically remains unchanged. The thermal energy absorption by convection of the UMC-PVT-SC increases. When wind speed reaches 4.4 m/s, the thermal energy absorption by photothermal conversion of the UMC-PVT-SC accounts for 42 % of the total heat gain. The thermal energy absorption by convection of the UMC-PVT-SC accounts for 70 %, and the thermal energy absorption by radiation of PV panel accounts for −12 %. With the increase of wind speed, the convective heat transfer between the microchannel tube lower surface and ambient air is enhanced, and thermal energy absorption by convection and its proportion increase. The temperature of the PV panel increases. As the temperature difference between the PV panel and the effective sky temperature increases, the radiation heat dissipation of PV panel increases. In addition, as wind speed increases, the convective heat transfer coefficient at the surface of the PV panel increases, but the temperature difference between the PV panel and the ambient temperature gradually decreases. Therefore, the thermal energy absorption by convection of the PV panel increases at first and then decreases. As solar radiation intensity remains at a given value, the thermal energy absorption by photothermal conversion of the UMC-PVT-SC basically remains unchanged and its ratio becomes less since the total heat gain increases.

As shown in Fig. 34, with the increase of wind speed from 0.4 m/s to 4.4 m/s, the heat gains of the condenser and UMC-PVT-SC, power consumption of compressor increase, and the increases of the heat gains are slightly larger than that of the power consumption of compressor, while the power generation merely changes. The pressure ratio gradually decreases. The heat gain of the condenser increases from 1128.0 W to 1445.0 W. The heat gain of the UMC-PVT-SC increases from 887.3 W to 1182.6 W. The power consumption of compressor increases from 240.7 W to 262.4 W. The power generation ranges from 140.3 W to 136.3 W. The pressure ratio decreases from 4.94 to 3.87. The increase in

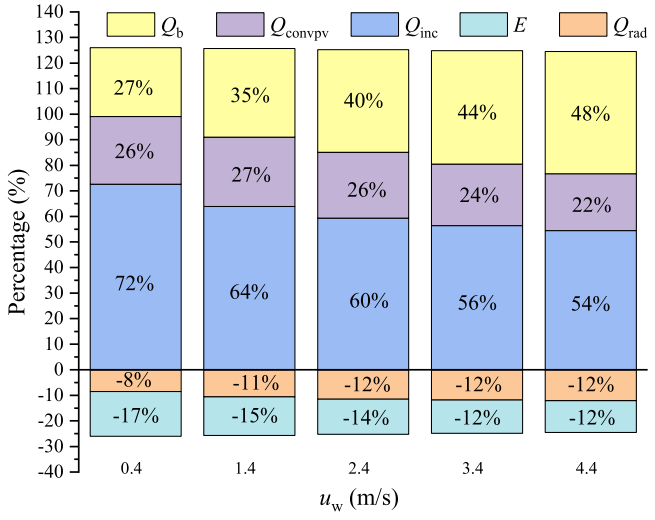

Fig. 32. Contribution rate of each heat source to heat gain of UMC-PVT-SC vs wind speed.

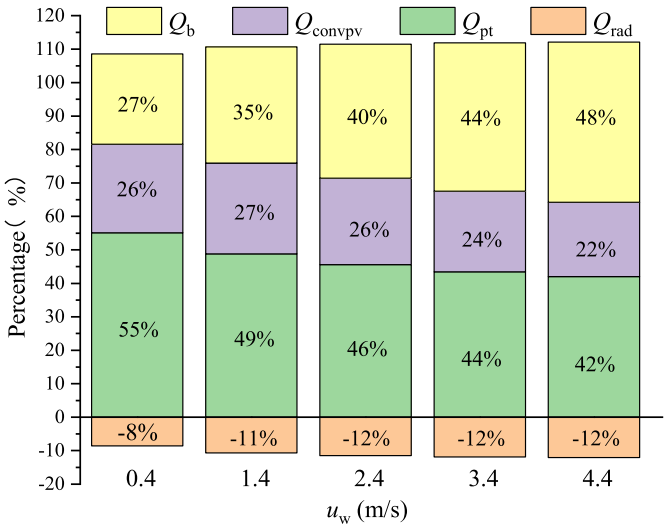

Fig. 33. Contribution rate of each heat source to heat gain of evaporator vs wind speed.

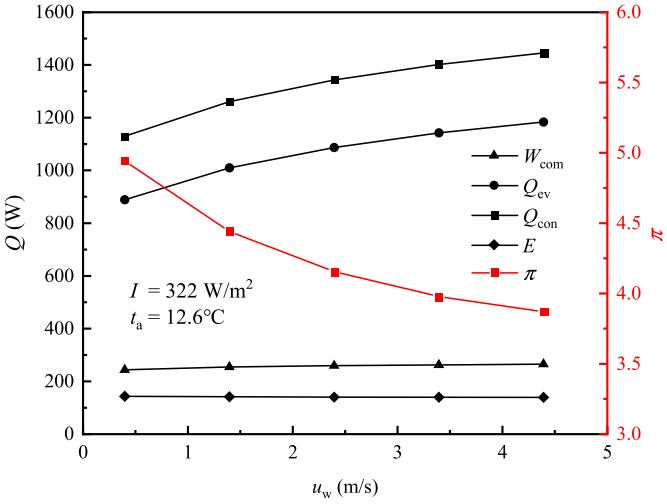

Fig. 34. Power generation, heat gain of condenser, heat gain of UMC-PVT-SC, compressor power consumption and pressure ratio vs wind speed.

wind speed promotes the overall heat transfer from the ambient air to refrigerant, leading to the increase of the thermal energy absorption between the UMC-PVT-SC and the ambient air by convection, and increases of the evaporation temperature and evaporation pressure. Since the effective sky temperature remains unchanged for a given ambient air temperature, the radiation heat dissipation between the PV cell and the sky increases, but its magnitude is smaller than the increase of the convection thermal energy absorption. The heat gain of the UMC-PVT-SC shows a gradually increasing trend. With the increase of wind speed, the system pressure gradually decreases, and the enthalpy difference between the inlet and outlet of the compressor decreases. The refrigerant mass flow rate gradually increases, whose increasing trend is larger than the decreasing trend of the enthalpy difference between the compressor inlet and outlet. Therefore, the power consumption gradually increases in a small range. The power generation of PV cell gradually decreases due to the temperature rise of the PV panel.

As shown in Fig. 35, with the increase of wind speed from 0.4 m/s to 4.4 m/s, the collector efficiency and overall energy efficiency of the UMC-PVT-SC gradually increase. COP_{HP} and COP_{pvt} increase. The water heating time gradually decreases. The electric efficiency decreases slightly. COP_{HP} increases from 4.85 to 5.77. COP_{pvt} increases from 6.43

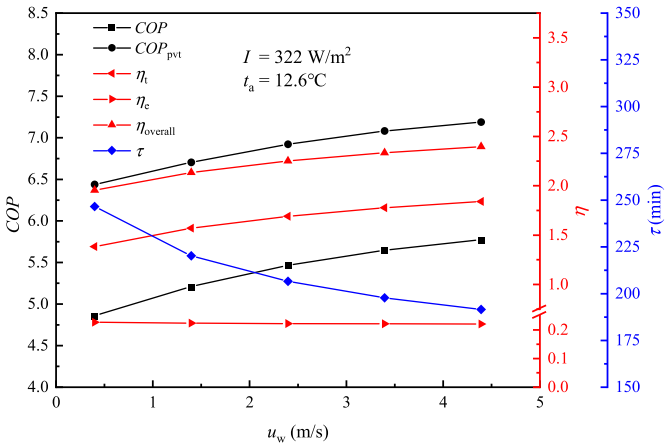

Fig. 35. Collector efficiency, electric efficiency, overall energy efficiency of the UMC-PVT-SC, heating time, *COP* and COP_{pvt} vs wind speed.

to 7.19. The collector efficiency increases from 1.378 to 1.836. The electric efficiency decreases from 0.2245 to 0.2181. The overall energy efficiency increases from 1.951 to 2.393. The water heating time decreases from 246.36 min to 191.20 min. As wind speed increases, the thermal energy absorption by convection of the UMC-PVT-SC increases gradually. Therefore, the heat gains of the UMC-PVT-SC and the condenser increases. The increase of the power consumption of the compressor is smaller than that of the heat gain of the condenser, so the COP_{HP} and COP_{pvt} increase. The heating capacity of the system is enhanced and the heating time is shortened. The electric efficiency decreases slightly due to the temperature rise of the PV panel. As wind speed increases, the heat absorbed by the UMC-PVT-SC increases. As the total amount of solar radiation received by the collector surface remains unchanged, the collector efficiency of the UMC-PVT-SC gradually increases, and the total energy efficiency of the system also increases simultaneously.

4.5. Analysis of operating performances of UMC-PVT-SC

According to the simulation results, during the operation of the UMC-PVT-SC, the ratio of the thermal energy obtained from solar radiation to that from ambient air is dynamically adjusted by the changing of the evaporation temperature of the heat pump system. In terms of electrical power generation, the refrigerant takes away the heat converted during electricity generation to control the temperature of the PV cell and improve the electricity generation efficiency.

As can be seen from Figs. 21, 27 and 33, the heat gain of UMC-PVT-SC is from multiple heat sources, i.e., the photothermal energy conversion, convection heat transfer, and radiation heat transfer. This is due to the micro-channel evaporator and uninsulated design of the PV/T components, where the larger heat exchange area of the micro-channel flat tubes allows the UMC-PVT-SC to achieve dual-source absorption of solar energy and thermal energy in air to cope with different weather conditions. According to the definition of collector efficiency of UMC-PVT-SC, the collector efficiency does not only reflect the ability of UMC-PVT-SC to absorb solar radiation but also reflect the performance of UMC-PVT-SC to obtain heat from the surrounding ambient air. Therefore, the thermal energy absorption performance of UMC-PVT-SC is significantly improved, which increases as solar radiation intensity increases at the ambient temperature of 12.6 °C. As solar radiation intensity increases, the thermal energy absorption by photothermal conversion of the UMC-PVT-SC and the evaporation temperature of solar collector increases, the thermal energy absorption by convection of the UMC-PVT-SC decreases, and the ratio of heat from solar radiation to that from air increases. As ambient temperature and wind speed increases, the thermal energy absorption by convection of the UMC-PVT-SC increases. The high flow boiling heat transfer of refrigerant in micro-channel tubes allows the collector to have an extremely fast response to temperature changes. Therefore, the UMC-PVT-SC shows a strong ability to adjust and adapt with the variations of the working conditions. In addition, the micro-channel flat tube array exhibits excellent heat uniformity performance, thereby enabling the UMC-PVT-SC to effectively absorb heat from PV panel, reduce the working temperature of PV cell, and improve the electric efficiency of the PV cell.

As can be seen from Fig. 23, when the solar radiation intensity is lower than 600 W/m^2, the collector efficiency of the UMC-PVT-SC is larger than unit and gradually increases. When the solar radiation intensity is 122 W/m^2 (low solar radiation condition), the heating time of the hot water storage tank is 212.2 min, the evaporation temperature drops to −0.7 °C, but the collector efficiency of UMC-PVT-SC reaches 4.31. This indicates that the UMC-PVT-SC can absorb more heat from the ambient air by reducing the evaporation temperature at lower solar radiation intensity to ensure the thermal energy absorption capacity. Therefore, the system can still operate at lower solar radiation intensity.

As can be seen from Fig. 29, when ambient temperature is higher than −7.5 °C, the collector efficiency of the UMC-PVT-SC is higher than unit, gradually increases with the increase of ambient temperature, and reaches the maximum value of 2.7 when ambient temperature is 32.6 °C. It is worth mentioning that when the system operates in the condition of very low ambient temperature below −7.5 °C, the collector efficiency of UMC-PVT-SC is lower than unit and decreases with the decrease of ambient temperature. For example, when ambient temperature is −18.6 °C, the collector efficiency is 0.718. This is because when ambient temperature is very low, the heat loss from the PV panel to the surroundings by convective and radiation heat transfer is larger than the incident solar energy on the PV panel surface.

4.6. Analysis of operation performances of DX-HPWH using UMC-PVT-SC

The DX-HPWH system using UMC-PVT-SC, named as UMC-PVT-HPWH, can make use of the photovoltaic/thermal energies and store both thermal and electric energies. The complementary utilization of energies ensures the high coefficient of performance. The COP_{HP} and COP_{pvt} of the UMC-PVT-HPWH in winter in Beijing are 5.54 and 7.00, respectively, under basic working conditions. The heat sources of the UMC-PVT-SC include solar radiation and ambient air. To achieve high-efficiency complementary for two heat sources, the ratio of the heat from solar radiation to that from ambient air can be dynamically adjusted by changing the evaporation temperature. Therefore, the coefficient of performance of the heat pump system can be improved.

As can be seen from Fig. 23, when solar radiation intensity is 122 W/m^2 (low solar radiation condition), the COP_{HP} and COP_{pvt} of the system are 5.36 and 5.92, respectively. As can be seen from Fig. 29, when the system operates at low ambient temperature of −18.6 °C, the COP_{HP} and COP_{pvt} of the system are 3.50 and 5.63, respectively. This shows that the performance coefficient of the system remains at an acceptable level in the low solar radiation condition or low ambient temperature condition.

As can be seen from Fig. 22, in winter, the power consumption of the compressor is 257.1 W and the PV cell power generation is 137.0 W. The system heating time is 202.76 min, the power consumption is 0.8687 kWh. The system power generation is 0.4631 kWh, which cannot meet the power required by the system operation. The average daily solar radiation duration in winter in Beijing is 10 h, so the system can generate electricity outside the running time and store the output electricity in the battery for the use of the system. Within 10 h, the system generates 1.3704 kWh of electricity, which can meet the system power consumption and form a comprehensive energy system with PV power as the main part and commercial power as the auxiliary part to realize the dual storage of thermoelectric power. The determination of PV panel area and component optimization have not been covered in this paper and will be further optimized in the future.

4.7. Comparison of proposed system with other solar direct-expansion heat pumps available in literature

The novel UMC-PVT-HPWH proposed in the present work can achieve thermal energy absorption from dual sources of solar radiation and ambient air without the need for an additional air-source evaporator. During nighttime or overcast weather conditions, the heat pump system operates in air-source mode. The electrical efficiency, collector efficiency, and overall efficiency of the collector can be improved. The complementary utilization of energies ensures the high coefficient of performance of the system using UMC-PVT-SC. Comparisons of efficiencies and coefficients of performance between the proposed system in the present work and other systems available in literature, under similar operating conditions, are given in Table 4.

5. Conclusions

In the present work, the DX-HPWH system integrated UMC-PVT-SC has been modelled and numerically simulated. The results for the system performance under different solar radiation intensity, ambient temperature and wind speed are presented and analyzed. The conclusions are drawn as follows:

(1) The uninsulated micro-channel solar collector demonstrates exceptionally good energy utilization of thermal energy from both solar radiation and ambient air due to its unique micro-channel structure and uninsulated design. The collector efficiency, electric efficiency and overall energy efficiency in winter in Beijing are 1.72, 0.2194 and 2.28, respectively. Even in the condition of low solar radiation intensity of 122 W/m^2 and ambient temperature of 12.6 °C, the collector efficiency, electric efficiency and overall energy efficiency are 4.31, 0.2218 and 4.87, respectively. Even in the condition of low ambient temperature of −18.6 °C and solar radiation intensity of 322 W/m^2, the collector efficiency, electric efficiency and overall energy efficiency are 0.718, 0.2442 and 1.341, respectively.

(2) The DX-HPWH system integrated with UMC-PVT-SC can achieve and maintain high COP_{HP} and COP_{pvt}. The COP_{HP} and COP_{pvt} in winter in Beijing are 5.54 and 7.00, respectively. Even in the low solar radiation intensity of 122 W/m^2 or low ambient temperature of −18.6 °C, the COP_{HP} and COP_{pvt} are 5.36 and 5.92, 3.50 and 5.63, respectively.

(3) As solar radiation intensity, ambient temperature and wind speed increase, the COP_{HP} and COP_{pvt} increase while the required operating time reduces. The solar radiation intensity shows the highest influence on the system performance. The COP_{pvt} at a solar radiation intensity of 1000 W/m^2 is 42.8 % higher than that at a solar radiation intensity of 122 W/m^2. The ambient temperature shows a moderate influence on the system performance. The COP_{pvt} at an ambient temperature of 32.6 °C is 37.5 % higher than that at an ambient temperature of −18.6 °C. The wind speed shows the lowest influence on the system performance. The COP_{pvt} at a wind speed of 4.4 m/s is 10.5 % higher than that at a wind speed of 0.4 m/s.

Table 4
Performance comparison between the proposed system in the present work and other systems available in literature.

Study	Working condition	Research approach	System configuration	η	COP
This work	I = 322 W/m^2 t_a = 12.6 °C	Simulation	DX-HPWH system based on UMC-PVT-SC	η_e = 16.3 % η_t = 170 % η_{pvt} = 212.9 %	COP_{HP} = 5.54 COP_{pvt} = 7
Abbas et al. [16]	I = 638 W/m^2 t_a = 23 °C	Experiment	A series -coupled PV/T-TC- SAHP system (with insulation layer)	η_e = 14.01 % η_t = 60.12 % η_{pvt} = 74.20 %	COP_{HP} = 6.01
Cai et al. [17]	I = 300 W/m^2 t_a = 10 °C	Simulation	HPWH system based on PV/T evaporator (with insulation layer) and air source evaporator	η_e = 15.36 % η_t = 44.16 % η_{pvt} = 84.6 %	–
Zhou et al. [25]	I = 606 W/m^2 t_a = 11.1 °C	Simulation	PV/T-DX-SAHP system based on micro-channels evaporator (with insulation layer)	η_e = 13.7 % η_t = 55 % η_{pvt} = 69.1 %	COP_{HP} = 5.0
Zhang et al. [26]	I = 609.4 W/m^2 t_a = 7.2 °C	Simulation	PV/T-SAHP system with MCHP and fin heat exchanger (with insulation layer)	η_e = 18 % η_t = 170 %	COP_{pvt} = 5.27
Yao et al. [39]	I = 190 W/m^2 t_a = 28.5 °C	Simulation	PV/T-SAHP system based on roll-bond evaporator	η_e = 17.16 % η_t = 47.60 %	COP_{pvt} = 4.37
Zhang et al. [40]	I = 1045 W/m^2 t_a = 31.1 °C	Experiment	PV/T-SAHP system with insulation layer	η_e = 13.6 % η_t = 26.42 % η_{pvt} = 62.49 %	COP_{HP} = 4.87

CRediT authorship contribution statement

Lidong Yang: Writing – original draft, Formal analysis, Data curation. **Qiang Gao:** Writing – original draft, Software, Formal analysis, Data curation. **Qiang Xu:** Resources, Investigation. **Liwei Yang:** Writing – review & editing, Visualization. **Rongji Xu:** Writing – review & editing, Methodology, Data curation, Conceptualization. **Hongbing Chen:** Validation, Formal analysis. **Huasheng Wang:** Writing – review & editing.

Declaration of competing interest

The authors declare that they have no known competing financial interests or personal relationships that could have appeared to influence the work reported in this paper.

Data availability

Data will be made available on request.

Acknowledgments

The present work was supported by the National Key R&D Program of China (No. 2020YFF0303904), National Natural Science Foundation of China (51506004), Beijing Municipal Science and Technology Project (Z231100006123014), Queen Mary University of London (201808060459) and Beijing University of Civil Engineering and Architecture Post Graduate Innovation Project (PG2024075).

Nomenclature

A	area, m^2
A_c	flow area or cross-sectional area, m^2
A_e	calibration area, 0.485 m^2
A_f	adiabatic factor
a	thermal diffusivity, m/s^2
a_{pv}	absorption rate
a^*	aspect ratio
Bd	Bond number
Bo	boiling number
COP	coefficient of performance
COP_{HP}	coefficient of performance of heat pump
COP_{pvt}	coefficient of performance of PV/thermal system
D	hydraulic diameter, m
E	photovoltaic cell power generation, W
F	fin efficiency
F_f	fluid-dependent parameter
Fr	Froude number
f	friction factor
G	mass flux, $kg/(m^2 \cdot s)$
g	acceleration due to gravity, m/s^2
H	micro-channel spacing, m
h	specific enthalpy, J/kg
I	solar radiation intensity, W/m^2
k	thermal conductivity, W/(m·K)
L	length, m
l	shaped size, m
M	molecular mass, kg/kmol
m	mass flow rate, kg/s
m_r	refrigerant mass flow rate, kg/s
Nu	Nusselt number
n	parameters in the definition of fin efficiency
P	wetted perimeter, m
p	pressure, kPa
p_{con}	condensation pressure, kPa
p_{crit}	critical pressure, kPa
p_{ev}	evaporation pressure, kPa
p_r	reduced pressure, kPa
Pr	Prandtl number
Q	heat exchange, W
Q_b	the thermal energy absorption by convection from the bottom surface of micro-channel tubes, W
Q_{conv}	the thermal energy absorption of the UMC-PVT-SC by convection, W
Q_{convpv}	the thermal energy absorption of PV panel by convection, W
Q_{ev}	the total thermal absorption of UMC-PVT-SC, W
Q_{inc}	the total incident solar energy on the PV panel surface, W
Q_{pt}	the thermal energy absorption of photothermal conversion of the UMC-PVT-SC, W
Q_{pv}	the thermal energy absorption of PV panel, W
Q_{rad}	the thermal energy absorption of PV panel by radiation, W
q	heat flux from channel wall to fluid, W/m^2
R	contact thermal resistance, $(m^2 \cdot K)/W$
s	height of monolithic micro-channel, m
t	Celsius temperature, °C
t_a	ambient air temperature, °C
t_{con}	condensation temperature, °C
t_{ev}	evaporation temperature, °C
t_{pv}	PV panel temperature, °C
T	absolute temperature, K
T_{rc}	the reference operating temperature, 298.15 K
T_{sky}	effective sky temperature, K
u_w	outdoor wind speed, m/s
W	power consumption, W
x	vapor quality
y	width of monolithic micro-channel, m

Greek symbols

α	volume expansion coefficient, 1/K
β_{rc}	the temperature coefficient, 0.9352/K
δ	thickness, m
ε	emissivity
η	efficiency
η_e	electric efficiency of UMC-PVT-SC
η_t	collector efficiency of the UMC-PVT-SC
η_{pvt}	overall energy efficiency of UMC-PVT-SC
η_{rc}	the electrical efficiency of PV cell under standard condition, 20.4 %
λ	thermal conductivity, W/(m·K)
μ	dynamic viscosity, Pa·s
μ_{lf}	the liquid dynamic viscosities valued at the fluid temperature, Pa·s
μ_{lw}	the liquid dynamic viscosities valued at the inner wall surface temperature, Pa·s
ξ	void fraction
π	compressor ratio
ρ	density, kg/m^3
σ	Boltzmann constant
σ_{fi}	film thickness, m
τ	time, s
τ_g	transmittance
ν	kinematic viscosity, m/s^2
χ	quality
Σ	mathematical operator for summation
Φ	two-phase multiplier

Subscripts

An	annular
a	ambient
b	bottom
cm	condenser micro-channel
con	condenser
conv	convection
convpv	convection of photovoltaic cell
com	compressor
eev	electronic expansion valve
ev	evaporator
ele	electricity
em	evaporator micro-channel
F	forced convection dominant
f	friction factor
G	gas
g	glass
HP	heat pump
i	i-th micro element
in	inlet
inc	incident solar radiation
iwe	inner wall of evaporator micro-channel
iwt	inner wall of hot water storage tank
j	j-th time step
L	liquid phase
Lo	liquid phase with total flow
Ls	liquid slug
n	total number of micro-elements divided
out	outlet
owc	outer wall of condenser micro-channel
owe	outer wall of evaporator micro-channel
owt	outer wall of hot water storage tank
pt	photothermal
pv	photovoltaic cell
pvt	photovoltaic/thermal module

r	refrigerant
rad	radiation
S	surface tension dominant
tk	hot water storage tank
tcs	thermal conductive silicone
tp	two-phase state
tpt	TPT membrane
u	upper
V	vapor phase
Vo	vapor phase with total flow
w	water
wl	micro-channel wall
z	total number of time step

References

[1] Danish Recep Ulucak. A revisit to the relationship between financial development and energy consumption: is globalization paramount? Energy 2021;227:120337.
[2] Shiwei Yu, Xing Hu, Li Longxi, Chen Hao. Does the development of renewable energy promote carbon reduction? Evidence from Chinese provinces. J Environ Manag 2020;268:110634.
[3] Moreno-Rodriguez A, Garcia-Hernando N, Gonzalez-Gil A, Izquierdo M. Experimental validation of a theoretical model for a direct-expansion solar-assisted heat pump applied to heating. Energy 2013;60:242–53.
[4] Sun Xiaolin, Dai Yanjun, Novakovic V, Wu J, Wang Ruzhu. Performance comparison of direct expansion solar-assisted heat pump and conventional air source heat pump for domestic hot water. Energy Proc 2015;70:394–401.
[5] Song Zhiying, Ji Jie, Cai Jingyong, Zhao Bin, Li Zhaomeng. Investigation on a direct-expansion solar-assisted heat pump with a novel hybrid compound parabolic concentrator/photovoltaic/fin evaporator. Appl Energy 2021;299:117279.
[6] Song Zhiying, Ji Jie, Zhang Yuzhe, Cai Jingyong, Li Zhaomeng. Comparative study on dual-source direct-expansion heat pumps based on different composite concentrating photovoltaic/fin evaporators. Appl Energy 2022;306:118073.
[7] Kong Xiangqiang, Wang Baigong, Shang Yanping, Li Jinyu, Ying Li. Influence of different regulation modes of compressor speed on the performance of direct-expansion solar-assisted heat pump water heater. Appl Therm Eng 2020;169:115007.
[8] Kong Xiangqiang, Zhang Maoyuan, Yang Yimeng, Ying Li, Wang Dechang. Comparative experimental analysis of direct-expansion solar-assisted heat pump water heaters using R134a and R290. Sol Energy 2020;203:187–96.
[9] Kong Xiangqiang, Ying Li, Lin Lin, Yang Yunguo. Modeling evaluation of a direct-expansion solar-assisted heat pump water heater using R410A. Int J Refrig 2017;76:136–46.
[10] Sabrina N Rabelo, Paulino Tiago F, Machado Luiz, Duarte Willian M. Economic analysis and design optimization of a direct expansion solar assisted heat pump. Sol Energy 2019;188:164–74.
[11] Zhang feng, Cai Jingyong, Jie Ji, Han Kedong, Ke Wei. Experimental investigation on the heating and cooling performance of a solar air composite heat source heat pump. Int J Refrig 2020;161:221–9.
[12] Yang Liwei, Hua Nan, Pu Jinhuan, Zhou Wenbin, Xu Rongji, Tong Yang, Belyayev Yerzhan, Wang Huasheng. Analysis of operation performance of three indirect expansion solar assisted air source heat pumps for domestic heating. Energy Convers Manag 2022;252:115061.
[13] Yang Liwei, Li Yan, Tong Yang, Wang Huasheng. Low temperature heating operation performance of a domestic heating system based on indirect expansion solar assisted air source heat pump. Sol Energy 2022;244:134–54.
[14] Yang Liwei, Xu Rongji, Hua Nan, Xia Yu, Zhou Wenbin, Yang Tong, Belyayev Yerzhan, Wang Huasheng. Review of the advances in solar-assisted air source heat pumps for the domestic sector. Energy Convers Manag 2021;247:114710.
[15] Vaishak S, Bhale Purnanand V. Photovoltaic/thermal-solar assisted heat pump system: current status and future prospects. Sol Energy 2019;189:268–84.
[16] Abbas Sajid, Zhou Jinzhi, Hassan Atazaz, Yuan Yanping, Yousuf Saima, Sun Yafen, Zeng Chao. Economic evaluation and annual performance analysis of a novel series-coupled PV/T and solar TC with solar direct expansion heat pump system: an experimental and numerical study. Renew Energy 2023;204:400–20.
[17] Cai Jingyong, Ji Jie, Wang Yunyun, Fang Zhou, Yu Bendong. A novel PV/T-air dual source heat pump water heater system: dynamic simulation and performance characterization. Energy Convers Manag 2017;148:635–45.
[18] Wu Jinshun, Zhang Xingxing, Shen Jingchun, Wu Yupeng, Connelly Karen, Tong Yang, Tang Llewellyn, Xiao Manxuan, Wei Yixuan, Jiang Ke, Chen Chao, Xu Peng, Wang Hong. A review of thermal absorbers and their integration methods for the combined solar photovoltaic/thermal (PV/T) modules. Renew Sustain Energy Rev 2017;75:839–54.
[19] Lu Shixiang, Liang Ruobing, Zhang Jili, Zhou Chao. Performance improvement of solar photovoltaic/thermal heat pump system in winter by employing vapor injection cycle. Appl Therm Eng 2019;155:135–46.
[20] Chen Hongbing, Niu Haoyu, Zhang Lei, Xiong Yaxuan, Zhai Huixing, Nie Jinzhe. Performance testing of a heat pipe PV/T heat pump system under different working modes. Int J Low Carbon Technol 2018;13:177–83.
[21] Chen Hongbing, Zhang Lei, Jie Pengfei, Xiong Yaxuan, Xu Peng, Zhai Huixing. Performance study of heat-pipe solar photovoltaic/thermal heat pump system. Appl Energy 2017;190:960–80.
[22] Huang Binghuan, Li Haiwang, Xia Shuangzhi, Xu Tiantong. Experimental investigation of the flow and heat transfer performance in micro-channel heat exchangers with cavities. Int J Heat Mass Tran 2020;159:120075.
[23] Kim S, Madawar I. Universal approach to predicting saturated flow boiling heat transfer in mini/micro-channels – part II: two-phase heat transfer coefficient. Int J Heat Mass Tran 2013;64:1239–56.
[24] Hajji Hassnia, Kolsi Lioua, Ghachem Kaouther, Maatki Chemseddine, Hussein Ahmed Kadhim, Borjini Mohamed Naceur. Numerical study of heat transfer and flow structure over a microscale backstep. Alex Eng J 2021;60(3):2759–68.
[25] Zhou Jinzhi, Ma Xiaoli, Zhao Xudong, Yuan Yanping, Yu Min, Li Jing. Numerical simulation and experimental validation of a micro-channel PV/T modules based direct-expansion solar heat pump system. Renew Energy 2020;145:1992–2004.
[26] Zhang Yuzhe, Ji Jie, Song Zhiying, Ke Wei, Xie Hao. Performance prediction on a novel dual-mode heat pump with a hybrid photovoltaic/micro-channel heat pipe/fin heat exchanger. Energy Convers Manag 2023;293:117505.
[27] Modjinou Mawufemo, Ji Jie, Yuan Weiqi, Fan Zhou, Sarah Holliday, Adeel Waqas, Zhao Xudong. Performance comparison of encapsulated PCM PV/T, microchannel heat pipe PV/T and conventional PV/T systems. Energy 2019;166:1249–66.
[28] Syed Muhammad Ammar, Chan Woo Park. Validation of the Gnielinski correlation for evaluation of heat transfer coefficient of enhanced tubes by non-linear regression model: an experimental study of absorption refrigeration system. Int Commun Heat Mass Tran 2020;118:104819.
[29] Fang Xiande, Qi Wu, Yuan Yulian. A general correlation for saturated flow boiling heat transfer in channels of various sizes and flow directions. Int J Heat Mass Tran 2016;107:972–81.
[30] Zhou Jinzhi, Ma Xiaoli, Zhao Xudong, Yuan Yanping, Yu Min, Li Jing. Numerical simulation and experimental validation of a micro-channel PV/T modules based direct-expansion solar heat pump system. Renew Energy 2020;145:1992–2004.
[31] Watmuff JH, Charters WWWS, Proctor D. Solar and wind induced external coefficients-Solar collectors. Cooperation Mediterraneenne Pour Lenergie Solaire 1977;1:56.
[32] Yin Ershuai, Li Qiang, Xuan Yimin. Optimal design method for concentrating photovoltaic-thermoelectric hybrid system. Appl Energy 2018;226:320–9.
[33] Nowak H. The sky temperature in net radiant heat loss calculations from low-sloped roofs. Infrared Phys 1989;29(2):231–2.
[34] Zhao Weiqiang, Li Shuhong, Zhang Xiaosong. Analysis of the operating characteristics of hybrid heat sources: heat pump water heater under variable conditions. Chem Ind Eng Prog 2017;36(11):3977–85.
[35] Jige Daisuke, Inoue Norihiro, Koyama Shigeru. Condensation of refrigerants in a multiport tube with rectangular minichannels. Int J Refrig 2016;67:202–13.
[36] Cai Jingyong, Jie Ji, Wang Yunyun, Fan Zhou, Bendong Yu. A novel PV/T-air dual source heat pump water heater system: dynamic simulation and performance characterization. Energy Convers Manag 2017;148:635–45.
[37] General Administration of Quality Supervision, Inspection and Quarantine of the People's Republic of China, Standardization Administration. Specifications of air source heat pump assisted domestic solar water heating systems GB/T 23889-2009. Beijing: Standards Press of China; 2010.
[38] Lu Shixiang, Liang Ruobing, Zhang Jili, Zhou Chao. Performance improvement of solar photovoltaic/thermal heat pump system in winter by employing vapor injection cycle. Applied Thermal Energy 2019;155:135–46.
[39] Yao Jian, Liu Wenjie, Zhao Yao, Dai Yanjun, Zhu Junjie, Novakovic Vojislav. Two-phase flow investigation in channel design of the roll-bond cooling component for solar assisted PVT heat pump application. Energy Convers Manag 2021;235:113988.
[40] Dong Zhang, Su Xinyue, Liu Pengfei, Hui Bo, Hou Gang, Liu Chunyang, Xu Baorui, Zhang Tao, An Zhoujian. Experiment study on startup characteristics and operation performance of PV/T solar assisted heat pump water heater system driven by direct current variable frequency compressor. Sol Energy 2023;263:111771.